

MATRIX EQUATION TECHNIQUES FOR CERTAIN EVOLUTIONARY PARTIAL DIFFERENTIAL EQUATIONS*

DAVIDE PALITTA†

Abstract. We show that the discrete operator stemming from the time and space discretization of evolutionary partial differential equations can be represented in terms of a single Sylvester matrix equation. A novel solution strategy that combines projection techniques with the full exploitation of the entry-wise structure of the involved coefficient matrices is proposed. The resulting scheme is able to efficiently solve problems with a tremendous number of degrees of freedom while maintaining a low storage demand as illustrated in several numerical examples.

Key words. Evolutionary PDEs, matrix equations, Sylvester equations, projection methods

AMS subject classifications. 65F30, 65M22, 65M06, 93C20

1. Introduction. The numerical treatment of partial differential equations (PDEs) often involves a first discretization phase which yields a discrete operator that needs to be inverted. In general, if a d -dimensional operator on a regular domain is discretized with n nodes in each direction, a common approach consists in writing the discrete problem as a large linear system

$$(1.1) \quad \mathcal{A}u = f, \quad \mathcal{A} \in \mathbb{R}^{n^d \times n^d},$$

so that well-established procedures, either direct or iterative, can be employed in the solution process. However, in many cases, the coefficient matrix \mathcal{A} in (1.1) is very structured and a different formulation of the algebraic problem in terms of a matrix equation can be employed. The matrix oriented formulation of the algebraic problems arising from the discretization of certain PDEs is not new. See, e.g., [42–44]. Nevertheless, only in the last decades the development of efficient solvers for large-scale matrix equations allows for a full exploitation of such reformulation also during the solution phase. See, e.g., [7, 20, 31], and [40] for a thorough presentation about solvers for linear matrix equations.

In this paper, we discuss time-dependent PDEs and we show that the aforementioned reformulation in terms of a matrix equation can be performed also for this class of operators. The model problem we have in mind is the heat equation

$$(1.2) \quad \begin{aligned} u_t &= \Delta u + f, & \text{in } \Omega \times (0, T], \\ u &= g, & \text{on } \partial\Omega, \\ u(x, 0) &= u_0(x), \end{aligned}$$

where $\Omega \subset \mathbb{R}^d$, $d = 1, 2, 3$, is a regular domain.

We discretize the problem (1.2) in both space and time, and, for sake of simplicity, we assume that a finite difference method with a uniform mesh is employed in the space discretization whereas we apply a backward differentiation formula (BDF) of order s , $s = 1, \dots, 6$, for the discretization in time.

If an “all-at-once” approach is considered, the algebraic problem arising from the discretization of (1.2) amounts to a linear system of the form (1.1) with $\mathcal{A} \in \mathbb{R}^{n^{d\ell} \times n^{d\ell}}$ where n is the number of nodes employed in each of the d space directions, d is the space dimension and ℓ is the number of time steps. As shown in [27], the $n^{d\ell} \times n^{d\ell}$ coefficient matrix \mathcal{A} possesses a Kronecker structure. While in [27] the authors exploit this Kronecker form to design an effective preconditioner for (1.1), we take advantage of the Kronecker structure to reformulate the algebraic problem in terms of a matrix equation and we show how timely projection techniques can be applied for its efficient solution.

The most common approximation spaces used in the solution of matrix equations by projection are the extended Krylov subspace

$$(1.3) \quad \mathbf{EK}_m^\square(A, B) := \text{Range}([B, AB, A^{-1}B, \dots, A^{m-1}B, A^{-m}B]), \quad A \in \mathbb{R}^{n \times n}, B \in \mathbb{R}^{n \times p}, p \ll n,$$

*Version of July 19, 2022.

†Research Group Computational Methods in Systems and Control Theory (CSC), Max Planck Institute for Dynamics of Complex Technical Systems, Sandtorstraße 1, 39106 Magdeburg, Germany. palitta@mpi-magdeburg.mpg.de

see, e.g., [19,38], and the more general rational Krylov subspace

$$(1.4) \quad \mathbf{K}_m^\square(A, B, \boldsymbol{\xi}) := \text{Range}([B, (A - \xi_2 I)^{-1} B, \dots, \prod_{i=2}^m (A - \xi_i I)^{-1} B]),$$

where $\boldsymbol{\xi} = [\xi_2, \dots, \xi_m]^T \in \mathbb{C}^{m-1}$. See, e.g., [9–11]. We thus consider only these spaces in our analysis.

Here is a synopsis of the paper. Assuming the backward Euler scheme, i.e., a BDF of order 1, is employed for the time integration, in section 2 we show how the all-at-once approach for the solution of (1.2) leads to a Sylvester matrix equation. An automatic incorporation of the boundary conditions for the matrix equation formulation is illustrated in section 3 while in section 4 the efficient solution of the obtained algebraic problem is discussed. In particular, in section 4.1 we present the new solution procedure for problems where only the space component of the discrete operator is reduced by projection onto a suitable subspace, i.e., we consider problems where the number of time steps ℓ is small, say $\ell = \mathcal{O}(10^3)$. For $d = 2, 3$, also the stiffness matrix arising from the discretization of the Laplace operator has a Kronecker structure that can be further exploited in the solution process as illustrated in section 4.1.1. At each iteration, the projection technique presented in section 4.1 requires the solution of a reduced equation and this task is one of most expensive parts of the entire procedure, especially for large ℓ . In section 4.2 we illustrate a novel strategy that dramatically decreases the cost of such inner solves. In section 4.3 we generalize the approach to the case of generic BDFs of order s , $s = 1, \dots, 6$. For the sake of simplicity, only the extended Krylov subspace (1.3) is considered in the discussion presented in section 4 but in section 5 we show how to easily adapt our new strategy when the rational Krylov subspace (1.4) is adopted as approximation space. The novel framework we present can be employed in the solution of many different PDEs and in section 6 we describe the solution process in case of time-dependent convection-diffusion equations. Several results illustrating the potential of our new methodology are reported in section 7 while our conclusions are given in section 8.

Throughout the paper we adopt the following notation. The matrix inner product is defined as $\langle X, Y \rangle_F = \text{trace}(Y^T X)$ so that the induced norm is $\|X\|_F^2 = \langle X, X \rangle_F$. The Kronecker product is denoted by \otimes while the operator $\text{vec} : \mathbb{R}^{n \times n} \rightarrow \mathbb{R}^{n^2}$ is such that $\text{vec}(X)$ is the vector obtained by stacking the columns of the matrix X one on top of each other. The identity matrix of order n is denoted by I_n . The subscript is omitted whenever the dimension of I is clear from the context. Moreover, e_i is the i -th basis vector of the canonical basis of \mathbb{R}^n while E_i denotes the i -th block of q columns of an identity matrix whose dimension depends on the adopted approximation space. More precisely, when the extended Krylov subspace (1.3) is employed, $q = 2 \cdot p$ while $q = p$ when the rational Krylov subspace (1.4) is selected. The brackets $[\cdot]$ are used to concatenate matrices of conforming dimensions. In particular, a Matlab-like notation is adopted and $[M, N]$ denotes the matrix obtained by putting M and N one next to the other. If $w \in \mathbb{R}^n$, $\text{diag}(w)$ denotes the $n \times n$ diagonal matrix whose i -th diagonal entry corresponds to the i -th component of w .

Given a suitable space \mathcal{K}_m ¹, we will always assume that a matrix $V_m \in \mathbb{R}^{n \times r}$, $\text{Range}(V_m) = \mathcal{K}_m$, has orthonormal columns and it is full rank so that $\dim(\mathcal{K}_m) = r$. Indeed, if this is not the case, deflation strategies to overcome the possible linear dependence of the basis vectors can be adopted as it is customary in block Krylov methods. See, e.g., [16, Section 8].

2. A matrix equation formulation. Assuming that the backward Euler scheme is employed for the time integration, if $\bar{\Omega}_h = \{\bar{x}_{i_d}\}$, $\bar{x}_{i_d} \in \mathbb{R}^d$, $\mathbf{i}_d = (i_1, \dots, i_d)^T \in \mathbb{N}^d$, $i_j = 1, \dots, n$ for all $j = 1, \dots, d$, denotes a uniform discretization of the closed domain $\bar{\Omega}$, with n equidistant points in each of the d spatial dimensions, and the time interval $[0, T]$ is discretized with $\ell + 1$ equidistant nodes $\{t_k\}_{k=0, \dots, \ell}$, then the discretization of (1.2) leads to

$$(2.1) \quad \frac{\mathbf{u}_k - \mathbf{u}_{k-1}}{\tau} + K_d \mathbf{u}_k = \mathbf{f}_k, \quad k = 1, \dots, \ell.$$

In (2.1), $K_d \in \mathbb{R}^{n^d}$ denotes the stiffness matrix arising from the finite difference discretization of the d -dimensional negative laplacian on $\bar{\Omega}_h$, $\tau = T/\ell$ is the time-step size, $\mathbf{f}_k \in \mathbb{R}^{n^d}$ collects all the space nodal values of f at time t_k , namely $f(x_{i_d}, t_k)$ for all $x_{i_d} \in \bar{\Omega}_h$, together with the boundary conditions, while \mathbf{u}_k gathers the approximations to the space nodal values of the solution u at time t_k , i.e., $u(x_{i_d}, t_k)$ for all $x_{i_d} \in \bar{\Omega}_h$ ².

¹ \mathcal{K}_m as in (1.3) or (1.4).

²We assume the entries of both \mathbf{f}_k and \mathbf{u}_k to be sorted following a lexicographic order on the multi-index \mathbf{i}_d for all $k = 1, \dots, \ell$.

As shown in [27], rearranging the terms in (2.1) and applying an all-at-once approach, we get the $n^d \ell \times n^d \ell$ linear systems

$$(2.2) \quad \underbrace{\begin{bmatrix} I_{n^d} + \tau K_d & & & \\ -I_{n^d} & I_{n^d} + \tau K_d & & \\ & \ddots & \ddots & \\ & & -I_{n^d} & I_{n^d} + \tau K_d \end{bmatrix}}_{=: \mathcal{A}} \begin{bmatrix} \mathbf{u}_1 \\ \mathbf{u}_2 \\ \vdots \\ \mathbf{u}_\ell \end{bmatrix} = \begin{bmatrix} \mathbf{u}_0 + \tau \mathbf{f}_1 \\ \tau \mathbf{f}_2 \\ \vdots \\ \tau \mathbf{f}_\ell \end{bmatrix},$$

where \mathbf{u}_0 collects the space nodal values of the initial condition u_0 .

The coefficient matrix \mathcal{A} in (2.2) can be written as $\mathcal{A} = I_\ell \otimes (I_{n^d} + \tau K_d) - \Sigma_1 \otimes I_{n^d}$ where

$$\Sigma_1 = \begin{bmatrix} 0 & & & \\ 1 & 0 & & \\ & \ddots & \ddots & \\ & & 1 & 0 \end{bmatrix} \in \mathbb{R}^{\ell \times \ell}.$$

Therefore, if $\mathbf{U} = [\mathbf{u}_1, \dots, \mathbf{u}_\ell] \in \mathbb{R}^{n^d \times \ell}$, the linear system (2.2) can be reformulated as

$$(2.3) \quad (I_{n^d} + \tau K) \mathbf{U} - \mathbf{U} \Sigma_1^T = \mathbf{u}_0 e_1^T + \tau [\mathbf{f}_1, \dots, \mathbf{f}_\ell].$$

Many numerical methods for the efficient solution of the Sylvester matrix equation (2.3) can be found in the literature, see, e.g., [40], and in section 4 we present a procedure based on projection.

In what follows we always assume that the matrix $[\mathbf{f}_1, \dots, \mathbf{f}_\ell]$ admits a low-rank representation, namely $[\mathbf{f}_1, \dots, \mathbf{f}_\ell] = F_1 F_2^T$, $F_1 \in \mathbb{R}^{n^d \times p}$, $F_2 \in \mathbb{R}^{\ell \times p}$, $p \ll \min\{n^d, \ell\}$. Roughly speaking, this can be justified by assuming the functions f and g to be *sufficiently smooth* in time so that \mathbf{f}_k does not differ too much from \mathbf{f}_{k+1} if the time-step size τ is sufficiently small. More precisely, if \mathbf{f}_k contains entries having an analytic extension in an open elliptic disc with foci 0 and T for all k , then the results in [21, Lemma 2.2] and [21, Corollary 2.3] can be adapted to demonstrate an exponential (superexponential in case of entire function) decay in the singular values of $[\mathbf{f}_1, \dots, \mathbf{f}_\ell]$. This can be done by simply transforming the interval $[-1, 1]$ used in [21, Lemma 2.2] in the interval $[0, T]$. With this assumption, equation (2.3) can be written as

$$(2.4) \quad (I_{n^d} + \tau K_d) \mathbf{U} - \mathbf{U} \Sigma_1^T = [\mathbf{u}_0, F_1] [e_1, \tau F_2]^T.$$

If a finite element method is employed for the space discretization, also a mass matrix M has to be taken into account and the matrix equation we have to deal with has the form

$$(2.5) \quad (M + \tau K_d) \mathbf{U} - M \mathbf{U} \Sigma_1^T = [M \mathbf{u}_0, F_1] [e_1, \tau F_2]^T.$$

See, e.g., [27]. The generalized Sylvester equation (2.5) can be easily transformed into a standard Sylvester equation by premultiplying by M^{-1} , see, e.g., [40, Section 7], and the procedure we are going to present in section 4 can be applied to

$$(I_{n^d} + \tau M^{-1} K_d) \mathbf{U} - \mathbf{U} \Sigma_1^T = [\mathbf{u}_0, M^{-1} F_1] [e_1, \tau F_2]^T.$$

3. Imposing the boundary conditions. Before showing how to efficiently solve equation (2.3) by projection, we make a step back and illustrate an automatic procedure for including the boundary conditions in the formulation (2.3). We first assume $d = 1$ in (1.2). The boundary nodes correspond to the entries of index i , $i = 1, n$, in each column of \mathbf{U} . Denoting by \mathcal{P}_1 the operator which selects only the boundary nodes, namely its entries are 1 for indexes corresponding to boundary nodes and 0 otherwise, for 1-dimensional problems we have

$$\mathcal{P}_1 = \begin{bmatrix} 1 & & & \\ & 0 & & \\ & & \ddots & \\ & & & 0 \\ & & & & 1 \end{bmatrix} = e_1 e_1^T + e_n e_n^T.$$

The operator $I + \tau K_1$ should act as the identity operator on the space boundary nodes which means that

$$(3.1) \quad \mathcal{P}_1(I + \tau K_1) = \mathcal{P}_1.$$

Therefore, if we define the matrix

$$(3.2) \quad \bar{K}_1 := \begin{bmatrix} 1/\tau & & \\ & \mathring{K}_1 & \\ & & 1/\tau \end{bmatrix} \in \mathbb{R}^{n \times n},$$

we can consider $I_n - \mathcal{P}_1 + \tau \bar{K}_1$ in place of $I_n + \tau K_1$ as left coefficient matrix in (2.3). In (3.2), the matrix $\mathring{K}_1 \in \mathbb{R}^{(n-2) \times n}$ corresponds to the discrete operator stemming from the selected finite difference scheme and acting only on the interior of $\bar{\Omega}_h$. Different choices with respect to the one in (3.2) can be considered to meet the constrain (3.1). For instance, we can select $\tilde{K}_1 := [\underline{0}^T; \mathring{K}_1; \underline{0}^T]$, $\underline{0}$ the zero vector of length n , and consider $I_n + \tau \tilde{K}_1$ as coefficient matrix. However, such a \tilde{K}_1 is not suitable for the solution process we are going to present in section 4 due to its singularity and the matrix \bar{K}_1 in (3.2) is thus preferred.

We now show how to select the right-hand side in (2.3) when the coefficient matrix is as in (3.2). We have

$$\mathcal{P}_1(I_n - \mathcal{P}_1 + \tau \bar{K}_1) \mathbf{U} - \mathcal{P}_1 \mathbf{U} \Sigma_1^T = \mathcal{P}_1(\mathbf{u}_0 e_1^T + \tau[\mathbf{f}_1, \dots, \mathbf{f}_\ell]),$$

so that

$$\begin{bmatrix} \mathbf{u}_1(1) & \mathbf{u}_2(1) - \mathbf{u}_1(1) & \cdots & \mathbf{u}_\ell(1) - \mathbf{u}_{\ell-1}(1) \\ 0 & 0 & & 0 \\ \vdots & \vdots & & \vdots \\ 0 & 0 & & 0 \\ \mathbf{u}_1(n) & \mathbf{u}_2(n) - \mathbf{u}_1(n) & \cdots & \mathbf{u}_\ell(n) - \mathbf{u}_{\ell-1}(n) \end{bmatrix} = \begin{bmatrix} u_0(x_1) + \tau \mathbf{f}_1(1) & \tau \mathbf{f}_2(1) & \cdots & \tau \mathbf{f}_\ell(1) \\ 0 & 0 & & 0 \\ \vdots & \vdots & & \vdots \\ 0 & 0 & & 0 \\ u_0(x_n) + \tau \mathbf{f}_1(n) & \tau \mathbf{f}_2(n) & \cdots & \tau \mathbf{f}_\ell(n) \end{bmatrix}.$$

Therefore, we can set $\mathbf{f}_1(1) = \mathbf{f}_1(n) = 0$ whereas $\mathbf{f}_k(j) = (g(x_j, t_k) - g(x_j, t_{k-1}))/\tau$, $k = 2, \dots, \ell$, $j = 1, n$.

A similar approach can be pursued also for 2- and 3-dimensional problems. In this cases, following the same ordering of the unknowns proposed in [31], it can be shown that the operator selecting the boundary nodes in \mathbf{U} has the form

$$\mathcal{P}_2 = \mathcal{P}_1 \otimes I_n + (I_n - \mathcal{P}_1) \otimes \mathcal{P}_1, \quad \mathcal{P}_3 = \mathcal{P}_1 \otimes I_n \otimes I_n + (I_n - \mathcal{P}_1) \otimes \mathcal{P}_1 \otimes I_n + (I_n - \mathcal{P}_1) \otimes (I_n - \mathcal{P}_1) \otimes \mathcal{P}_1,$$

for $d = 2, 3$ respectively.

It is well-known that also K_d possesses a Kronecker structure. In particular,

$$K_2 = K_1 \otimes I_n + I_n \otimes K_1, \quad K_3 = K_1 \otimes I_n \otimes I_n + I_n \otimes K_1 \otimes I_n + I_n \otimes I_n \otimes K_1.$$

The most natural choice for imposing the boundary conditions is thus to select

$$\bar{K}_2 = \bar{K}_1 \otimes I_n + I_n \otimes \bar{K}_1, \quad \bar{K}_3 = \bar{K}_1 \otimes I_n \otimes I_n + I_n \otimes \bar{K}_1 \otimes I_n + I_n \otimes I_n \otimes \bar{K}_1,$$

and use $I_{n^2} - \mathcal{P}_2 + \tau \bar{K}_2$ and $I_{n^3} - \mathcal{P}_3 + \tau \bar{K}_3$ as coefficient matrices in (2.3). Notice that $I_{n^d} - \mathcal{P}_d = \bigotimes_{i=1}^d (I_n - \mathcal{P}_1)$.

A direct computation shows that

$$(3.3) \quad \mathcal{P}_2 \left(\bigotimes_{i=1}^2 (I_n - \mathcal{P}_1) + \tau \bar{K}_2 \right) = \mathcal{P}_2 + \mathcal{P}_1 \otimes (I_n - \mathcal{P}_1) \bar{K}_1 + (I_n - \mathcal{P}_1) \bar{K}_1 \otimes \mathcal{P}_1 = \mathcal{P}_2 + \mathcal{L}_2,$$

and

$$(3.4) \quad \begin{aligned} \mathcal{P}_3 \left(\bigotimes_{i=1}^3 (I_n - \mathcal{P}_1) + \tau \bar{K}_3 \right) &= \mathcal{P}_3 + (\mathcal{P}_1 \otimes I_n \otimes I_n) (I_n \otimes \bar{K}_1 \otimes I_n + I_n \otimes I_n \otimes \bar{K}_1) \\ &\quad + ((I_n - \mathcal{P}_1) \otimes \mathcal{P}_1 \otimes I_n) (\bar{K}_1 \otimes I_n \otimes I_n + I_n \otimes I_n \otimes \bar{K}_1) \\ &\quad + ((I_n - \mathcal{P}_1) \otimes (I_n - \mathcal{P}_1) \otimes \mathcal{P}_1) (\bar{K}_1 \otimes I_n \otimes I_n + I_n \otimes \bar{K}_1 \otimes I_n) \\ &= \mathcal{P}_3 + \mathcal{L}_3. \end{aligned}$$

Therefore the extra terms $\mathcal{L}_2, \mathcal{L}_3$ in (3.3)-(3.4) must be taken into account when constructing the right-hand side $\mathbf{u}_0 e_1^T + \tau[\mathbf{f}_1, \dots, \mathbf{f}_\ell]$, and the relation

$$\mathcal{P}_d \left(\bigotimes_{i=1}^d (I_n - \mathcal{P}_1) + \tau \bar{K}_d \right) \mathbf{U} - \mathcal{P}_d \mathbf{U} \Sigma_1^T = \mathcal{P}_d (\mathbf{u}_0 e_1^T + \tau[\mathbf{f}_1, \dots, \mathbf{f}_\ell]), \quad d = 2, 3,$$

i.e.,

$$\mathcal{P}_d \mathbf{U} + \mathcal{L}_d \mathbf{U} - \mathcal{P}_d \mathbf{U} \Sigma_1^T = \mathcal{P}_d (\mathbf{u}_0 e_1^T + \tau[\mathbf{f}_1, \dots, \mathbf{f}_\ell]), \quad d = 2, 3,$$

must hold. See, e.g., [31, Section 3] for a similar construction.

To conclude, after imposing the boundary conditions and recalling the discussion at the end of section 2, the Sylvester equation we need to solve is

$$(3.5) \quad \left(\bigotimes_{i=1}^d (I_n - \mathcal{P}_1) + \tau \bar{K}_d \right) \mathbf{U} - \mathbf{U} \Sigma_1^T = [\mathbf{u}_0, F_1][e_1, \tau F_2], \quad d = 1, 2, 3,$$

and in the next section we illustrate its efficient solution by projection.

4. The extended Krylov subspace method. In this section we show how to effectively solve equation (3.5) by means of the extended Krylov subspace method. An efficient implementation of this algorithm called K-PIK for large-scale Lyapunov equations can be found in [38] whereas its extension to the solution of Sylvester equations has been proposed in [6]. In the next section we suppose that the number ℓ of time steps is moderate, say $\ell = \mathcal{O}(10^3)$, so that only a left projection, i.e., a reduction of the space discrete operator, has to be performed. See, e.g., [32, Section 5.2] or [40, Section 4.3] for some details about projection methods for this problem setting.

In section 4.2 we then suppose that a large number of time steps ℓ is employed in the time discretization so that a naive solution of the inner problems stemming from our projection technique is not feasible. By exploiting the structure of Σ_1 we propose a valid remedy to overcome this numerical issue.

4.1. Left projection. The extended Krylov subspace method constructs an approximation $U_m = V_m Y_m \in \mathbb{R}^{n^d \times \ell}$ where the $2m(p+1)$ columns of V_m form an orthonormal basis of the extended Krylov subspace $\mathbf{EK}_m^\square(\bar{K}_d, [\mathbf{u}_0, F_1])$, so that $\text{Range}(V_m) = \mathbf{EK}_m^\square(\bar{K}_d, [\mathbf{u}_0, F_1])$. Notice that we use only \bar{K}_d in the definition of the space instead of the whole coefficient matrix $\bigotimes_{i=1}^d (I_n - \mathcal{P}_1) + \tau \bar{K}_d$. Indeed, all the spectral information about the spatial operator are collected in \bar{K}_d . See, e.g., [39] for a similar strategy in the context of extended Krylov subspace methods for shifted linear systems.

The basis $V_m = [\mathcal{V}_1, \dots, \mathcal{V}_m] \in \mathbb{R}^{n^d \times 2m(p+1)}$ can be constructed by the extended Arnoldi procedure presented in [38] while the matrix $Y_m \in \mathbb{R}^{2m(p+1) \times \ell}$ can be computed, e.g., by imposing a Galerkin condition on the residual matrix $R_m := (\bigotimes_{i=1}^d (I_n - \mathcal{P}_1) + \tau \bar{K}_d) U_m - U_m \Sigma_1^T - [\mathbf{u}_0, F_1][e_1, \tau F_2]^T$. This Galerkin condition can be written as

$$V_m^T R_m = 0,$$

so that Y_m is the solution of the reduced Sylvester equation

$$(4.1) \quad (\mathcal{I}_m + \tau T_m) Y_m - Y_m \Sigma_1^T = E_1 \boldsymbol{\gamma} [e_1, \tau F_2]^T,$$

where $T_m = V_m^T \bar{K}_d V_m$, $\mathcal{I}_m = V_m^T (\bigotimes_{i=1}^d (I_n - \mathcal{P}_1)) V_m$ and $[\mathbf{u}_0, F_1] = V_1 \boldsymbol{\gamma}$, $\boldsymbol{\gamma} \in \mathbb{R}^{2(p+1) \times (p+1)}$. In exact arithmetic, the matrix T_m can be cheaply computed by the recursion formulas presented in [38]. However, from our numerical experience, computing an explicit projection of \bar{K}_d leads to a better representation of the boundary conditions in the projected problem (4.1), and thus in the solution U_m as well, in spite of a moderate computational extra cost. The recursion formulas in [38] probably suffers the presence of $1/\tau$ in the definition (3.2) of \bar{K}_1 , especially for very small τ .

An explicit projection has to be performed also to construct \mathcal{I}_m . However, the particular structure of $\bigotimes_{i=1}^d (I_n - \mathcal{P}_1)$ makes this task affordable in terms of number of operations. For instance, if $d = 1$, we have

$$\mathcal{I}_m = V_m^T (I_n - \mathcal{P}_1) V_m = V_m^T (I_n - e_1 e_1^T - e_n e_n^T) V_m = I_{2m(p+1)} - (V_m^T e_1)(V_m^T e_1)^T - (V_m^T e_n)(V_m^T e_n)^T,$$

so that only the small matrices $(V_m^T e_1)(V_m^T e_1)^T$, $(V_m^T e_n)(V_m^T e_n)$ have to be computed. Moreover, at the following iteration, $(V_{m+1}^T e_i) = [V_m^T e_i; \mathcal{V}_{m+1}^T e_i]$ and this structure can be exploited to further reduce the cost of computing \mathcal{I}_m . A similar discussion shows that the computation of \mathcal{I}_m is a minor cost also for $d = 2, 3$.

Due to its small dimension, equation (4.1) can be solved by means of general-purposed dense solvers for Sylvester equations like the Bartels-Stewart method [2] or the Hessenberg-Schur method presented in [14] which may be particularly appealing in our context due to the lower Hessenberg pattern of Σ_1^T . See also [4, Section 3]. However, the structure of (4.1) allows for a cheaper alternative. If $Y_m = [y_1, \dots, y_\ell]$, then equation (4.1) can be written as

$$[(\mathcal{I}_m + \tau T_m)y_1, (\mathcal{I}_m + \tau T_m)y_2 - y_1, \dots, (\mathcal{I}_m + \tau T_m)y_\ell - y_{\ell-1}] = E_1 \boldsymbol{\gamma} [e_1, \tau F_2]^T.$$

Since $\bigotimes_{i=1}^d (I_n - \mathcal{P}_1) + \tau \bar{K}_d$ is positive definite, also $\mathcal{I}_m + \tau T_m$ is positive definite and thus invertible for every m . Writing the relation above column-wise we get

$$(4.2) \quad \begin{aligned} y_1 &= (\mathcal{I}_m + \tau T_m)^{-1} E_1 \boldsymbol{\gamma} [e_1, \tau F_2]^T e_1, \\ y_j &= (\mathcal{I}_m + \tau T_m)^{-1} (E_1 \boldsymbol{\gamma} [e_1, \tau F_2]^T e_j + y_{j-1}), \quad j = 2, \dots, \ell. \end{aligned}$$

This means that the columns of Y_m can be computed by sequentially solving ℓ small linear systems with the same coefficient matrix $\mathcal{I}_m + \tau T_m$ whose factorization can be computed only once at each iteration.

Once Y_m is computed, it is easy to show that the Frobenius norm of the residual matrix R_m can be cheaply evaluated as

$$(4.3) \quad \|R_m\|_F = \tau \|E_{m+1}^T \underline{T}_m Y_m\|_F,$$

where $\underline{T}_m = V_{m+1}^T \bar{K}_d V_m$. See, e.g., [32, Section 5.2].

In Algorithm 4.1 the extended Krylov subspace method for equation (3.5) is summarized.

Algorithm 4.1 Extended Krylov subspace method for (3.5) - left projection.

input : $\bar{K}_d \in \mathbb{R}^{n^d \times n^d}$, $\Sigma_1 \in \mathbb{R}^{\ell \times \ell}$, $\mathbf{u}_0 \in \mathbb{R}^{n^d}$, $F_1 \in \mathbb{R}^{n^d \times p}$, $F_2 \in \mathbb{R}^{\ell \times p}$, m_{\max} , $\epsilon > 0$, $\tau > 0$.
output: V_m, Y_m s.t. $U_m = V_m Y_m \approx \mathbf{U}$ approximate solution to (3.5).

- 1 Compute $\delta = \|[\mathbf{u}_0, F_1][e_1, \tau F_2]^T\|_F$
 - 2 Perform economy-size QR, $[\mathbf{u}_0, F_1, \bar{K}_d^{-1}[\mathbf{u}_0, F_1]] = [\mathcal{V}_1^{(1)}, \mathcal{V}_1^{(2)}][\boldsymbol{\gamma}, \boldsymbol{\theta}]$, $\boldsymbol{\gamma}, \boldsymbol{\theta} \in \mathbb{R}^{2(p+1) \times (p+1)}$
 - 3 Set $V_1 = [\mathcal{V}_1^{(1)}, \mathcal{V}_1^{(2)}]$
 - for** $m = 1, 2, \dots$, *till* m_{\max} **do**
 - 4 Compute next basis block \mathcal{V}_{m+1} as in [38] and set $V_{m+1} = [V_m, \mathcal{V}_{m+1}]$
 - 5 Update $T_m = V_m^T \bar{K}_d V_m$ and $\mathcal{I}_m = V_m^T \left(\bigotimes_{i=1}^d (I_n - \mathcal{P}_1) \right) V_m$
 - 6 Compute Y_m as in (4.2)
 - 7 **if** $\tau \|E_{m+1}^T \underline{T}_m Y_m\|_F \leq \delta \cdot \epsilon$ **then**
 | **Return** V_m and Y_m
 - end**
 - end**
-

Notice that the initial residual norm $\|[\mathbf{u}_0, F_1][e_1, \tau F_2]^T\|_F$ in line 1 of Algorithm 4.1 can be computed at low cost exploiting the properties of the Frobenius norm and the trace operator. Indeed,

$$\begin{aligned} \delta^2 &= \|[\mathbf{u}_0, F_1][e_1, \tau F_2]^T\|_F^2 = \|\mathbf{u}_0 e_1^T\|_F^2 + \tau^2 \|F_1 F_2^T\|_F^2 + 2\tau \langle \mathbf{u}_0 e_1^T, F_1 F_2^T \rangle_F \\ &= \mathbf{u}_0^T \mathbf{u}_0 + \tau^2 \cdot \text{trace}((F_1^T F_1)(F_2^T F_2)) + 2\tau \mathbf{f}_1^T \mathbf{u}_0. \end{aligned}$$

In many cases the dimension of the final space $\mathbf{E}K_m^\square(\bar{K}_d, [\mathbf{u}_0, F_1])$, namely the number of columns of V_m , turns out to be much smaller than ℓ . See section 7. Therefore, to reduce the memory demand of Algorithm 4.1, we suggest to store only V_m and Y_m and not to explicitly assemble the solution matrix $U_m = V_m Y_m \in \mathbb{R}^{n^d \times \ell}$. If desired, one can access to the computed approximation to the solution u at time t_k by simply performing $V_m(Y_m e_k)$.

4.1.1. Structured space operators. As already mentioned, for 2- and 3-space-dimensional problems, i.e., (1.2) with $d = 2, 3$, also the stiffness matrix \bar{K}_d possesses a Kronecker structure. See section 3.

In principle, one can apply the strategy proposed in section 4.1 and build the space $\mathbf{EK}_m^\square(\bar{K}_d, [\mathbf{u}_0, F_1])$. However, if u_0, f and g in (1.2) are separable functions in the space variables, the Kronecker structure of \bar{K}_2 and \bar{K}_3 can be exploited in the basis construction. More precisely, only d subspaces of \mathbb{R}^n can be computed instead of one subspace of \mathbb{R}^{n^d} leading to remarkable reductions in both the computational cost and the storage demand of the overall solution process. See, e.g., [20]. The structure we study in this section is sometimes referred to as *Laplace-like* structure. Such a structure is at the basis of the *tensorized* Krylov approach presented in [20] but it has been exploited also in [25] to derive an ADI iteration tailored to certain high dimensional problems.

We first assume $d = 2$ and then extend the approach to the case of $d = 3$. If $\bar{\Omega}_h$ consists in n equidistant points in each direction (x_i, y_j) , $i, j = 1, \dots, n$, and $u_0 = \phi_{u_0}(x)\psi_{u_0}(y)$, then we can write

$$\mathbf{u}_0 = \boldsymbol{\phi}_{u_0} \otimes \boldsymbol{\psi}_{u_0},$$

where $\boldsymbol{\phi}_{u_0} = [\phi_{u_0}(x_1), \dots, \phi_{u_0}(x_n)]^T$, and $\boldsymbol{\psi}_{u_0} = [\psi_{u_0}(y_1), \dots, \psi_{u_0}(y_n)]^T$.

Similarly, if $f = \phi_f(x, t)\psi_f(y, t)$, $g = \phi_g(x, t)\psi_g(y, t)$, a generic column \mathbf{f}_k of the right-hand side in (2.3) can be written as

$$\mathbf{f}_k = \boldsymbol{\phi}_{f,k} \otimes \boldsymbol{\psi}_{f,k} + \boldsymbol{\phi}_{g,k} \otimes \boldsymbol{\psi}_{g,k},$$

with

$$\begin{aligned} \boldsymbol{\phi}_{f,k} &= [\phi_f(x_1, t_k), \dots, \phi_f(x_n, t_k)]^T, & \boldsymbol{\psi}_{f,k} &= [\psi_f(y_1, t_k), \dots, \psi_f(y_n, t_k)]^T, \\ \boldsymbol{\phi}_{g,k} &= [\phi_g(x_1, t_k), \dots, \phi_g(x_n, t_k)]^T, & \boldsymbol{\psi}_{g,k} &= [\psi_g(y_1, t_k), \dots, \psi_g(y_n, t_k)]^T. \end{aligned}$$

We further assume that the low-rank factorization $[\mathbf{f}_1, \dots, \mathbf{f}_\ell] = F_1 F_2^T$, $F_1 \in \mathbb{R}^{n^2 \times p}$, $F_2 \in \mathbb{R}^{\ell \times p}$, $p \ll \ell$, is such that the separability features of the functions f and g are somehow preserved. In other words, we assume that we can write

$$[\mathbf{f}_1, \dots, \mathbf{f}_\ell] = (\Phi_f \otimes \Psi_f) F_2^T,$$

where $\Phi_f \in \mathbb{R}^{n \times q}$, $\Psi_f \in \mathbb{R}^{n \times r}$, $qr = p$. Notice that this construction is not hard to meet in practice. See, e.g., section 7.

With the assumptions above, it has been shown in [20] how the construction of a *tensorized* Krylov subspace is very convenient. In particular, we can compute the space $\mathbf{EK}_m^\square(\bar{K}_1, [\boldsymbol{\phi}_{u_0}, \Phi_f]) \otimes \mathbf{EK}_m^\square(\bar{K}_1, [\boldsymbol{\psi}_{u_0}, \Psi_f])$ instead of $\mathbf{EK}_m^\square(\bar{K}_2, [\mathbf{u}_0, F_1])$.

The construction of $\mathbf{EK}_m^\square(\bar{K}_1, [\boldsymbol{\phi}_{u_0}, \Phi_f])$, $\mathbf{EK}_m^\square(\bar{K}_1, [\boldsymbol{\psi}_{u_0}, \Psi_f])$ is very advantageous in terms of both number of operations and memory requirements compared to the computation of $\mathbf{EK}_m^\square(\bar{K}_2, [\mathbf{u}_0, F_1])$. For instance, only multiplications and solves with the $n \times n$ matrix \bar{K}_1 are necessary while the orthogonalization procedures only involves vectors of length n . Moreover, at iteration m , we need to store the two matrices $Q_m \in \mathbb{R}^{n \times 2m(q+1)}$, $\text{Range}(Q_m) = \mathbf{EK}_m^\square(\bar{K}_1, [\boldsymbol{\phi}_{u_0}, \Phi_f])$, and $W_m \in \mathbb{R}^{n \times 2m(r+1)}$, $\text{Range}(W_m) = \mathbf{EK}_m^\square(\bar{K}_1, [\boldsymbol{\psi}_{u_0}, \Psi_f])$, so that only $2m(q+r+2)$ vectors of length n are allocated instead of the $2m(p+1)$ vectors of length n^2 the storage of V_m requires. Moreover, the construction of the bases W_m and Q_m can be carried out in parallel.

Even if we construct the matrices W_m and Q_m instead of V_m , the main framework of the extended Krylov subspace method remains the same. We look for an approximate solution of the form $U_m = (W_m \otimes Q_m) Y_m$ where the $4m^2(q+1)(r+1) \times \ell$ matrix Y_m is computed by imposing a Galerkin condition on the residual matrix $R_m = \left(\bigotimes_{i=1}^2 (I_n - \mathcal{P}_1) + \tau(\bar{K}_1 \otimes I_n + I_n \otimes \bar{K}_1) \right) (W_m \otimes Q_m) Y_m - (W_m \otimes Q_m) Y_m \Sigma_1^T - [\boldsymbol{\phi}_{u_0} \otimes \boldsymbol{\psi}_{u_0}, \Phi \otimes \Psi][e_1, \tau F_2]^T$. Such Galerkin condition can be written as

$$(W_m^T \otimes Q_m^T) R_m = 0,$$

so that Y_m is the solution of the reduced Sylvester equation

$$(4.4) \quad (\mathcal{I}_m \otimes \mathcal{J}_m + \tau(T_m \otimes I_{2m(q+1)} + I_{2m(r+1)} \otimes H_m)) Y_m - Y_m \Sigma_1^T = (E_1 \boldsymbol{\alpha} \otimes E_1 \boldsymbol{\beta}) [e_1, \tau F_2]^T,$$

where $T_m = W_m^T \bar{K}_1 W_m$, $H_m = Q_m^T \bar{K}_1 Q_m$, $\mathcal{I}_m = W_m^T (I_n - \mathcal{P}_1) W_m$, $\mathcal{J}_m = Q_m^T (I_n - \mathcal{P}_1) Q_m$, $[\boldsymbol{\phi}_{u_0}, \Phi_f] = Q_1 \boldsymbol{\alpha}$, $\boldsymbol{\alpha} \in \mathbb{R}^{2(q+1) \times (q+1)}$ and $[\boldsymbol{\psi}_{u_0}, \Psi_f] = W_1 \boldsymbol{\beta}$, $\boldsymbol{\beta} \in \mathbb{R}^{2(r+1) \times (r+1)}$.

As before, the ℓ columns of Y_m can be computed by solving ℓ linear systems with the same coefficient matrix $\mathcal{I}_m \otimes \mathcal{J}_m + \tau(T_m \otimes I_{2m(q+1)} + I_{2m(p+1)} \otimes H_m)$.

The cheap residual norm computation (4.3) has not a straightforward counterpart of the form $\|R_m\|_F = \tau \|E_{m+1}^T(\underline{T}_m \otimes I_{2m(q+1)} + I_{2m(r+1)} \otimes \underline{H}_m)Y_m\|_F$, $\underline{T}_m = W_{m+1}^T \bar{K}_1 W_m$, $\underline{H}_m = Q_{m+1}^T \bar{K}_1 Q_m$, in our current setting. A different though cheap procedure for computing the residual norm at low cost is derived in the next proposition.

PROPOSITION 4.1. *At the m -th iteration of the extended Krylov subspace method, the residual matrix $R_m = \left(\bigotimes_{i=1}^2 (I_n - \mathcal{P}_1) + \tau(\bar{K}_1 \otimes I_n + I_n \otimes \bar{K}_1)\right) (W_m \otimes Q_m)Y_m - (W_m \otimes Q_m)Y_m \Sigma_1^T - [\phi_{u_0} \otimes \psi_{u_0}, \Phi_f \otimes \Psi_f][e_1, \tau F_2]^T$ is such that*

$$(4.5) \quad \|R_m\|_F^2 = \tau^2 \left(\| (E_{m+1}^T \underline{T}_m \otimes I_{2m(q+1)}) Y_m \|_F^2 + \| (I_{2m(r+1)} \otimes E_{m+1}^T \underline{H}_m) Y_m \|_F^2 \right),$$

where $\underline{T}_m := W_{m+1}^T \bar{K}_1 W_m$ and $\underline{H}_m := Q_{m+1}^T \bar{K}_1 Q_m$.

Proof. If $Q_m = [Q_1, \dots, Q_m]$, $Q_i \in \mathbb{R}^{n \times 2(q+1)}$, $W_m = [W_1, \dots, W_m]$, $W_i \in \mathbb{R}^{n \times 2(r+1)}$, for the extended Krylov subspaces $\mathbf{EK}_m^\square(\bar{K}_1, [\phi_{u_0}, \Phi_f])$, $\mathbf{EK}_m^\square(\bar{K}_1, [\psi_{u_0}, \Psi_f])$ the Arnoldi relations

$$\bar{K}_1 Q_m = Q_m H_m + Q_{m+1} E_{m+1}^T \underline{H}_m,$$

and

$$\bar{K}_1 W_m = W_m T_m + W_{m+1} E_{m+1}^T \underline{T}_m,$$

hold. Since Y_m solves (4.4), we have

$$\begin{aligned} R_m &= \left(\bigotimes_{i=1}^2 (I_n - \mathcal{P}_1) + \tau(\bar{K}_1 \otimes I_n + I_n \otimes \bar{K}_1) \right) (W_m \otimes Q_m)Y_m - (W_m \otimes Q_m)Y_m \Sigma_1^T \\ &\quad - [\phi_{u_0} \otimes \psi_{u_0}, \Phi_f \otimes \Psi_f][e_1, \tau F_2]^T \\ &= (W_m \otimes Q_m) \left((\mathcal{I}_m \otimes \mathcal{J}_m + \tau(T_m \otimes I_{2m(q+1)} + I_{2m(p+1)} \otimes H_m)) Y_m - Y_m \Sigma_1^T - (E_1 \alpha \otimes E_1 \beta)[e_1, \tau F_2]^T \right) \\ &\quad + \tau (W_{m+1} E_{m+1}^T \underline{T}_m \otimes Q_m + W_m \otimes Q_{m+1} E_{m+1}^T \underline{H}_m) Y_m \\ &= \tau (W_{m+1} E_{m+1}^T \underline{T}_m \otimes Q_m + W_m \otimes Q_{m+1} E_{m+1}^T \underline{H}_m) Y_m. \end{aligned}$$

Therefore,

$$\begin{aligned} \|R_m\|_F^2 &= \tau^2 \| (W_{m+1} E_{m+1}^T \underline{T}_m \otimes Q_m + W_m \otimes Q_{m+1} E_{m+1}^T \underline{H}_m) Y_m \|_F^2 \\ &= \tau^2 \left(\| (W_{m+1} E_{m+1}^T \underline{T}_m \otimes Q_m) Y_m \|_F^2 + \| (W_m \otimes Q_{m+1} E_{m+1}^T \underline{H}_m) Y_m \|_F^2 \right. \\ &\quad \left. + \langle (W_{m+1} E_{m+1}^T \underline{T}_m \otimes Q_m) Y_m, (W_m \otimes Q_{m+1} E_{m+1}^T \underline{H}_m) Y_m \rangle_F \right) \\ &= \tau^2 \left(\| (W_{m+1} \otimes Q_m) (E_{m+1}^T \underline{T}_m \otimes I_{2m(q+1)}) Y_m \|_F^2 + \| (W_m \otimes Q_{m+1}) (I_{2m(r+1)} \otimes E_{m+1}^T \underline{H}_m) Y_m \|_F^2 \right) \\ &= \tau^2 \left(\| (E_{m+1}^T \underline{T}_m \otimes I_{2m(q+1)}) Y_m \|_F^2 + \| (I_{2m(r+1)} \otimes E_{m+1}^T \underline{H}_m) Y_m \|_F^2 \right), \end{aligned}$$

where we have exploited the orthogonality of the bases. \square

The variant of Algorithm 4.1 that benefits from the separable structure of the data is summarized in Algorithm 4.2.

Once again, the Frobenius norm δ at the beginning of Algorithm 4.2 can be cheaply computed by exploiting both the low-rank and the Kronecker structure of $[\phi_{u_0} \otimes \psi_{u_0}, \Phi_f \otimes \Psi_f][e_1, \tau F_2]^T$.

Having Q_m , W_m and Y_m at hand, we can compute the approximation to the solution u at time t_k by performing $\text{vec}(Q_m \bar{Y}_{m,k} W_m^T)$ where $\bar{Y}_{m,k} \in \mathbb{R}^{2m(q+1) \times 2m(r+1)}$ is such that $\text{vec}(\bar{Y}_{m,k}) = Y_m e_k$.

For 3-space-dimensional problems with separable data we can follow the same approach. If,

$$\mathbf{u}_0 = \phi_{u_0} \otimes \psi_{u_0} \otimes \mathbf{v}_{u_0}, \text{ and } [\mathbf{f}_1, \dots, \mathbf{f}_\ell] = (\Phi_f \otimes \Psi_f \otimes \Upsilon_f) F_2^T,$$

then we can compute the subspaces $\mathbf{EK}_m^\square(\bar{K}_1, [\phi_{u_0}, \Phi_f])$, $\mathbf{EK}_m^\square(\bar{K}_1, [\psi_{u_0}, \Psi_f])$ and $\mathbf{EK}_m^\square(\bar{K}_1, [\mathbf{v}_{u_0}, \Upsilon_f])$ instead of $\mathbf{EK}_m^\square(\bar{K}_3, [\mathbf{u}_0, F_1])$. The derivation of the method follows the same exact steps as before along with straightforward technicalities and we thus omit it here.

Algorithm 4.2 Extended Krylov subspace method for (3.5) - left projection, separable data, $d = 2$.

input : $\bar{K}_1 \in \mathbb{R}^{n \times n}$, $\Sigma_1 \in \mathbb{R}^{\ell \times \ell}$, $\phi_{u_0}, \psi_{u_0} \in \mathbb{R}^n$, $\Phi_f \in \mathbb{R}^{n \times q}$, $\Psi_f \in \mathbb{R}^{n \times r}$, $F_2 \in \mathbb{R}^{\ell \times p}$, $m_{\max}, \epsilon > 0, \tau > 0$.

output: Q_m, W_m, Y_m s. t. $U_m = (W_m \otimes Q_m)Y_m \approx \mathbf{U}$ approximate solution to (3.5).

- 1 Compute $\delta = \|\phi_{u_0} \otimes \psi_{u_0}, \Phi_f \otimes \Psi_f\|_{[e_1, \tau F_2]^T}^T$
 - 2 Perform economy-size QR, $[\phi_{u_0}, \Phi_f, \bar{K}_1^{-1}[\phi_{u_0}, \Phi_f]] = [Q_1^{(1)}, Q_1^{(2)}][\alpha, \theta]$, $\alpha, \theta \in \mathbb{R}^{2(q+1) \times (q+1)}$,
 $[\psi_{u_0}, \Psi_f, \bar{K}_1^{-1}[\psi_{u_0}, \Psi_f]] = [\mathcal{W}_1^{(1)}, \mathcal{W}_1^{(2)}][\beta, \xi]$, $\beta, \xi \in \mathbb{R}^{2(r+1) \times (r+1)}$
 - 3 Set $Q_1 = [Q_1^{(1)}, Q_1^{(2)}]$ and $W_1 = [\mathcal{W}_1^{(1)}, \mathcal{W}_1^{(2)}]$
 - for** $m = 1, 2, \dots$, **till** m_{\max} **do**
 - 4 Compute next basis blocks Q_{m+1}, W_{m+1} as in [38] and set $Q_{m+1} = [Q_m, Q_{m+1}]$, $W_{m+1} = [W_m, W_{m+1}]$
 - 5 Update $H_m = Q_m^T K_1 Q_m$, $T_m = W_m^T K_1 W_m$, $\mathcal{I}_m = W_m^T (I_n - \mathcal{P}_1) W_m$ and $\mathcal{J}_m = Q_m^T (I_n - \mathcal{P}_1) Q_m$
 - 6 Compute Y_m as in (4.4)
 - 7 **if** $\tau \sqrt{\| (E_{m+1}^T \mathcal{I}_m \otimes I_{2m(q+1)}) Y_m \|_F^2 + \| (I_{2m(r+1)} \otimes E_{m+1}^T \mathcal{H}_m) Y_m \|_F^2} \leq \delta \cdot \epsilon$ **then**
| **Return** Q_m, W_m and Y_m
end
- end**
-

4.2. Efficient inner solves. One of the computational bottlenecks of Algorithm 4.1 is the solution of the inner problems (4.1). For large ℓ , this becomes the most expensive step of the overall solution process. Therefore, especially for problems that require a fine time grid, a more computational appealing alternative to the solution of the ℓ linear systems in (4.2) must be sought.

In principle, one may think to generate a second approximation space in order to reduce also the time component of the discrete operator in (3.5), in agreement with standard procedures for Sylvester equations. See, e.g., [40, Section 4.4.1]. However, no extended Krylov subspace can be generated by Σ_1 due to its singularity. A different option may be to generate the polynomial Krylov subspace $\mathbf{K}_k^\square(\Sigma_1, [e_1, F_2]) = \text{Range}([[e_1, F_2], \Sigma_1 [e_1, F_2], \dots, \Sigma_1^{k-1} [e_1, F_2]])$. Nevertheless, this space is not very informative as $\text{Ker}(\Sigma_1) = \text{span}\{e_1\}$ and the action of Σ_1 on a vector $v = (v_1, \dots, v_\ell)^T \in \mathbb{R}^\ell$ only consists in a permutation of its components of the form $\Sigma_1 v = (0, v_1, \dots, v_{\ell-1})^T$ so that $\Sigma_1^k v = (0, \dots, 0, v_1, \dots, v_{\ell-k})^T$, $k \leq \ell$. Alternatively, one can try to apply an ADI iteration tailored to Sylvester equations [5]. However, the shift selection for the *right* coefficient matrix Σ_1^T may be tricky.

The matrix Σ_1 is such that

$$(4.6) \quad \Sigma_1 = C_1 - e_1 e_\ell^T, \quad C_1 = \begin{bmatrix} 0 & & & & 1 \\ 1 & 0 & & & \\ & & \ddots & & \\ & & & \ddots & \\ & & & & 1 & 0 \end{bmatrix} \in \mathbb{R}^{\ell \times \ell}.$$

This relation has been exploited in [27] to design an effective preconditioner for (1.1).

We can use (4.6) to transform equation (3.5) in a *generalized Sylvester equation* of the form

$$\left(\bigotimes_{i=1}^d (I_n - \mathcal{P}_1) + \tau \bar{K}_d \right) \mathbf{U} - \mathbf{U} C_1^T + \mathbf{U} e_\ell e_1^T = [\mathbf{u}_0, F_1][e_1, \tau F_2],$$

and the extended Krylov subspace $\mathbf{E}\mathbf{K}_k^\square(C_1, [e_1, F_2])$ may be employed in the solution process thanks to the low rank of the term $\mathbf{U} e_\ell e_1^T$ as proposed in [18]. However, useful spectral information are difficult to generate also in $\mathbf{E}\mathbf{K}_k^\square(C_1, [e_1, F_2])$ since C_1 is a permutation matrix.

We take advantage of the relation (4.6) in a different manner. At each iteration m of Algorithm 4.1, the projected equation (4.2) can be written as

$$(4.7) \quad (\mathcal{I}_m + \tau T_m) Y_m - Y_m C_1^T + Y_m e_\ell e_1^T = E_1 \gamma [e_1, \tau F_2]^T.$$

Since the Krylov space dimension is assumed to be small, we can compute the eigendecomposition of the coefficient matrix $\mathcal{I}_m + \tau T_m$, namely $\mathcal{I}_m + \tau T_m = S_m \Lambda_m S_m^{-1}$, $\Lambda_m = \text{diag}(\lambda_1, \dots, \lambda_{2m(p+1)})$ whereas, thanks

to its circulant structure, C_1 can be diagonalized by the fast Fourier transform (FFT), i.e., $C_1 = \mathcal{F}^{-1}\Pi\mathcal{F}$, $\Pi = \text{diag}(\mathcal{F}(C_1 e_1))$, where \mathcal{F} denotes the discrete Fourier transform matrix. See, e.g., [15, Equation (4.7.10)].

Pre and postmultiplying equation (4.7) by S_m^{-1} and \mathcal{F}^T respectively, we get

$$(4.8) \quad \Lambda_m \tilde{Y}_m - \tilde{Y}_m \Pi + \tilde{Y}_m (\mathcal{F}^{-T} e_\ell) (\mathcal{F} e_1)^T = S_m^{-1} E_1 \gamma (\mathcal{F}[e_1, \tau F_2])^T, \quad \tilde{Y}_m := S_m^{-1} Y_m \mathcal{F}^T.$$

The Kronecker form of equation (4.8) is

$$(I_\ell \otimes \Lambda_m - \Pi \otimes I_{2m(p+1)} + (\mathcal{F} e_1 \otimes I_{2m(p+1)}) (\mathcal{F}^{-T} e_\ell \otimes I_{2m(p+1)})^T) \text{vec}(\tilde{Y}_m) = \text{vec}(S_m^{-1} E_1 \gamma (\mathcal{F}[e_1, \tau F_2])^T).$$

Denoting by $L := I_\ell \otimes \Lambda_m - \Pi \otimes I_{2m(p+1)} \in \mathbb{R}^{2m(p+1)\ell \times 2m(p+1)\ell}$, $M := \mathcal{F} e_1 \otimes I_{2m(p+1)}$, $N := \mathcal{F}^{-T} e_\ell \otimes I_{2m(p+1)} \in \mathbb{R}^{2m(p+1)\ell \times 2m(p+1)}$, and applying the Sherman-Morrison-Woodbury formula [15, Equation (2.1.4)] we can write

$$(4.9) \quad \text{vec}(\tilde{Y}_m) = L^{-1} \text{vec}(S_m^{-1} E_1 \gamma (\mathcal{F}[e_1, \tau F_2])^T) - L^{-1} M (I_{2m(p+1)} + N^T L^{-1} M)^{-1} N^T L^{-1} \text{vec}(S_m^{-1} E_1 \gamma (\mathcal{F}[e_1, \tau F_2])^T).$$

With \tilde{Y}_m at hand, we can recover Y_m by simply performing $Y_m = S_m \tilde{Y}_m \mathcal{F}^{-T}$.

We are thus left with deriving a strategy for the computation of \tilde{Y}_m that should not require the explicit construction of L , M and N to be efficient. In what follows \odot denotes the Hadamard (element-wise) product.

Denoting by $\mathcal{H} \in \mathbb{R}^{2m(p+1)\ell}$ the matrix whose (i, j) -th element is given by $1/(\lambda_i - e_j^T (\mathcal{F}(C_1 e_1)))$, $i = 1, \dots, 2m(p+1)$, $j = 1, \dots, \ell$, since L is diagonal, we can write

$$L^{-1} \text{vec}(S_m^{-1} E_1 \gamma (\mathcal{F}[e_1, \tau F_2])^T) = \text{vec}(\mathcal{H} \odot (S_m^{-1} E_1 \gamma (\mathcal{F}[e_1, \tau F_2])^T)),$$

so that

$$N^T L^{-1} \text{vec}(S_m^{-1} E_1 \gamma (\mathcal{F}[e_1, \tau F_2])^T) = (\mathcal{H} \odot (S_m^{-1} E_1 \gamma (\mathcal{F}[e_1, \tau F_2])^T)) \mathcal{F}^{-T} e_\ell.$$

We now have a closer look at the matrix $N^T L^{-1} M$ in (4.9). The (i, j) -th entry of this matrix can be written as

$$(4.10) \quad \begin{aligned} e_i^T N^T L^{-1} M e_j &= e_i^T (\mathcal{F}^{-T} e_\ell \otimes I_{2m(p+1)})^T L^{-1} (\mathcal{F} e_1 \otimes I_{2m(p+1)}) e_j = \text{vec}(e_i e_\ell^T \mathcal{F}^{-1})^T L^{-1} \text{vec}(e_j e_1^T \mathcal{F}^T) \\ &= \text{vec}(e_i e_\ell^T \mathcal{F}^{-1})^T \text{vec}(\mathcal{H} \odot (e_j e_1^T \mathcal{F}^T)) = \langle \mathcal{H} \odot (e_j e_1^T \mathcal{F}^T), e_i e_\ell^T \mathcal{F}^{-1} \rangle_F \\ &= \text{trace}(\mathcal{F}^{-T} e_\ell e_i^T (\mathcal{H} \odot (e_j e_1^T \mathcal{F}^T))) = e_i^T (\mathcal{H} \odot (e_j e_1^T \mathcal{F}^T)) \mathcal{F}^{-T} e_\ell. \end{aligned}$$

Note the abuse of notation in the derivation above: e_i, e_j denote the canonical basis vectors of $\mathbb{R}^{2m(p+1)}$ whereas e_1, e_ℓ the ones of \mathbb{R}^ℓ .

An important property of the Hadamard product says that for any real vectors x, y and matrices A, B of conforming dimensions, we can write $x^T (A \odot B) y = \text{trace}(\text{diag}(x) A \text{diag}(y) B^T)$. By applying this result to (4.10), we get

$$(4.11) \quad \begin{aligned} e_i^T N^T L^{-1} M e_j &= \text{trace}(\text{diag}(e_i) \mathcal{H} \text{diag}(\mathcal{F}^{-T} e_\ell) \mathcal{F} e_1 e_j^T) = e_j^T \text{diag}(e_i) \mathcal{H} (\mathcal{F}^{-T} e_\ell \odot \mathcal{F} e_1) \\ &= e_j^T e_i e_i^T \mathcal{H} (\mathcal{F}^{-T} e_\ell \odot \mathcal{F} e_1) = \delta_{i,j} e_i^T \mathcal{H} (\mathcal{F}^{-T} e_\ell \odot \mathcal{F} e_1), \end{aligned}$$

where $\delta_{i,j}$ denotes the Kronecker delta, i.e., $\delta_{i,i} = 1$ and $\delta_{i,j} = 0$ otherwise. Equation (4.11) says that $N^T L^{-1} M$ is a diagonal matrix such that $N^T L^{-1} M = \text{diag}(\mathcal{H} (\mathcal{F}^{-T} e_\ell \odot \mathcal{F} e_1))$.

The vector $w := M (I_{2m(p+1)} + N^T L^{-1} M)^{-1} N^T L^{-1} \text{vec}(S_m^{-1} E_1 \gamma (\mathcal{F}[e_1, \tau F_2])^T)$ in (4.8) can thus be computed by performing

$$w = \text{vec} \left(\left((I_{2m(p+1)} + \text{diag}(\mathcal{H} (\mathcal{F}^{-T} e_\ell \odot \mathcal{F} e_1)))^{-1} (\mathcal{H} \odot (S_m^{-1} E_1 \gamma (\mathcal{F}[e_1, \tau F_2])^T)) \mathcal{F}^{-T} e_\ell \right) e_1^T \mathcal{F}^T \right).$$

The linear solve $L^{-1} w$ can be still carried out by exploiting the Hadamard product and the matrix \mathcal{H} as

$$L^{-1} w = \text{vec} \left(\mathcal{H} \odot \left(\left((I_{2m(p+1)} + \text{diag}(\mathcal{H} (\mathcal{F}^{-T} e_\ell \odot \mathcal{F} e_1)))^{-1} (\mathcal{H} \odot (S_m^{-1} E_1 \gamma (\mathcal{F}[e_1, \tau F_2])^T)) \mathcal{F}^{-T} e_\ell \right) e_1^T \mathcal{F}^T \right) \right).$$

To conclude, the matrix Y_m can be computed by

$$(4.12) \quad Y_m = S_m (Z - W) \mathcal{F}^{-T}, \quad \text{where} \quad \begin{aligned} Z &= \mathcal{H} \odot (S_m^{-1} E_1 \gamma (\mathcal{F}[e_1, \tau F_2])^T), \\ W &= \mathcal{H} \odot \left(\left((I_{2m(p+1)} + \text{diag}(\mathcal{H} (\mathcal{F}^{-T} e_\ell \odot \mathcal{F} e_1)))^{-1} Z \mathcal{F}^{-T} e_\ell \right) e_1^T \mathcal{F}^T \right), \end{aligned}$$

and no Kronecker products are involved in such a computation.

The computation of Y_m by (4.12) requires $\mathcal{O}(8m^3(p+1)^3 + (\log \ell + 4m^2(p+1)^2)\ell)$ floating point operations (flops) that has to be compared with the $\mathcal{O}(8m^3(p+1)^3 + 4m^2(p+1)^2\ell)$ flops needed to calculate Y_m by (4.2). Even though the presence of the FFT makes the asymptotic cost of (4.12) slightly larger than the one of (4.2), performing (4.12) is usually much faster than (4.2) in terms of actual computational time. Indeed, no for loops are required in (4.12) while efficient BLAS 3 operations can be exploited.

The discrete Fourier transform matrix \mathcal{F} is never explicitly assembled and in all the experiments reported in section 7 its action and the action of its inverse have been performed by means of the Matlab function `fft` and `ifft` respectively.

We would like to point out that the novel strategy presented in this section can be applied as a direct solver to equation (3.5) whenever the eigendecomposition of $\bigotimes_{i=1}^d (I_n - \mathcal{P}_1) + \tau \bar{K}_d$ can be computed, e.g., if (1.2) is discretized on a coarse spatial grid.

4.3. Multistep methods. If a BDF of order s is employed for the time discretization, with the same notation of section 2, equation (2.1) has to be replaced by

$$(4.13) \quad \frac{\mathbf{u}_k - \sum_{j=1}^s \alpha_j \mathbf{u}_{k-j}}{\tau \beta} + K_d \mathbf{u}_k = \mathbf{f}_k,$$

where $\alpha_j = \alpha_j(s)$, $\beta = \beta(s) \in \mathbb{R}$ are the coefficients defining the selected BDF. See Table 4.1³. It has been proved that for $s > 6$ the BDFs become unstable, see, e.g., [1, Section 5.2.3], and we thus restrict ourselves to the case of $s \leq 6$.

Table 4.1: Coefficients for the BDF of order s for $s \leq 6$. See, e.g., [1, Table 5.3].

| s | β | α_1 | α_2 | α_3 | α_4 | α_5 | α_6 |
|-----|---------|------------|------------|------------|------------|------------|------------|
| 1 | 1 | 1 | | | | | |
| 2 | 2/3 | 4/3 | -1/3 | | | | |
| 3 | 6/11 | 18/11 | -9/11 | 2/11 | | | |
| 4 | 12/25 | 48/25 | -36/25 | 16/25 | -3/25 | | |
| 5 | 60/137 | 300/137 | -300/137 | 200/137 | -75/137 | 12/137 | |
| 6 | 60/147 | 360/147 | -450/147 | 400/147 | -225/147 | 72/147 | -10/147 |

Following the discussion of section 2, the discrete problem coming from an all-at-once approach for (4.13) can be formulated in terms of the following Sylvester equation

$$(4.14) \quad (I + \tau \beta K_d) \mathbf{U} - \mathbf{U} \left(\sum_{j=1}^s \alpha_j \Sigma_j^T \right) = \mathbf{u}_0 e_1^T + \tau \beta [\mathbf{f}_1, \dots, \mathbf{f}_\ell],$$

where Σ_j denotes the $\ell \times \ell$ zero matrix having ones only in the j -th subdiagonal.

We still assume that the right-hand side in (4.14) admits a low-rank representation. In particular, $[\mathbf{f}_1, \dots, \mathbf{f}_\ell] = F_1 F_2^T$. Noticing that the boundary conditions can be imposed as described in section 3 provided

$$\bar{K}_1 = \begin{bmatrix} 1/(\tau \beta) & & \\ & \bar{K}_1 & \\ & & 1/(\tau \beta) \end{bmatrix},$$

the matrix equation we need to solve has the form

$$(4.15) \quad \left(\bigotimes_{i=1}^d (I_n - \mathcal{P}_1) + \tau \beta \bar{K}_d \right) \mathbf{U} - \mathbf{U} \left(\sum_{j=1}^s \alpha_j \Sigma_j^T \right) = [\mathbf{u}_0, F_1][e_1, \tau \beta F_2]^T, \quad d = 1, 2, 3.$$

³To have a consistent notation in the equations (4.14) and (3.5), we have changed sign to the α_j 's with respect to the values listed in [1, Table 5.3].

The left projection for the space operator can be still carried out as illustrated in section 4.1 and the employment of a BDF of order s , $1 < s \leq 6$, only affects the inner problem formulation. Equation (4.1) must be replaced by

$$(4.16) \quad (\mathcal{I}_m + \tau\beta T_m)Y_m - Y_m \left(\sum_{j=1}^s \alpha_j \Sigma_j^T \right) = E_1 \boldsymbol{\gamma} [e_1, \tau\beta F_2]^T.$$

Once Y_m is computed, the residual norm can be cheaply evaluated by

$$\|R_m\|_F = \tau\beta \|E_{m+1}^T \underline{T}_m Y_m\|_F.$$

As in the case of $s = 1$, the solution of equation (4.16) may be very expensive, especially for large ℓ , and an efficient procedure for the calculation of Y_m is thus necessary. The solution scheme we are going to derive takes inspiration from the method discussed in section 4.2. Indeed, we observe that

$$(4.17) \quad \sum_{j=1}^s \alpha_j \Sigma_j = C_s - [e_1, \dots, e_s] \boldsymbol{\alpha}_s [e_{\ell-s+1}, \dots, e_\ell]^T, \quad \boldsymbol{\alpha}_s = \begin{bmatrix} \alpha_s & \cdots & \cdots & \alpha_1 \\ & \alpha_s & \cdots & \alpha_2 \\ & & \ddots & \vdots \\ & & & \alpha_s & \alpha_{s-1} \\ & & & & \alpha_s \end{bmatrix} \in \mathbb{R}^{s \times s},$$

where $C_s \in \mathbb{R}^{\ell \times \ell}$ is circulant and can be thus diagonalized by the FFT, namely $C_s = \mathcal{F}^{-1} \Pi_s \mathcal{F}$, $\Pi_s = \text{diag}(\mathcal{F}(C_s e_1))$. Following section 4.2, we can write

$$\text{vec}(\tilde{Y}_m) = L^{-1} \text{vec}(S_m^{-1} E_1 \boldsymbol{\gamma} (\mathcal{F}[e_1, \tau\beta F_2])^T) - L^{-1} M (I_{2ms(p+1)} + N^T L^{-1} M)^{-1} N^T L^{-1} \text{vec}(S_m^{-1} E_1 \boldsymbol{\gamma} (\mathcal{F}[e_1, \tau\beta F_2])^T),$$

where now $L := I_\ell \otimes \Lambda_m - \Pi_s \otimes I_{2m(p+1)} \in \mathbb{R}^{2m(p+1) \times 2m(p+1)}$ and $M := \mathcal{F}[e_1, \dots, e_s] \otimes I_{2m(p+1)}$, $N := \mathcal{F}^{-T}[e_{\ell-s+1}, \dots, e_\ell] \boldsymbol{\alpha}_s^T \otimes I_{2m(p+1)} \in \mathbb{R}^{2m(p+1)\ell \times 2ms(p+1)}$. As before, the action of L^{-1} can be carried out by exploiting the matrix \mathcal{H} and the Hadamard product. In particular,

$$L^{-1} \text{vec}(S_m^{-1} E_1 \boldsymbol{\gamma} (\mathcal{F}[e_1, \tau\beta F_2])^T) = \text{vec}(\mathcal{H} \odot (S_m^{-1} E_1 \boldsymbol{\gamma} (\mathcal{F}[e_1, \tau\beta F_2])^T)),$$

and

$$N^T L^{-1} \text{vec}(S_m^{-1} E_1 \boldsymbol{\gamma} (\mathcal{F}[e_1, \tau\beta F_2])^T) = \text{vec}((\mathcal{H} \odot (S_m^{-1} E_1 \boldsymbol{\gamma} (\mathcal{F}[e_1, \tau\beta F_2])^T)) \mathcal{F}^{-T}[e_{\ell-s+1}, \dots, e_\ell] \boldsymbol{\alpha}_s^T).$$

The inspection of the entries of the matrix $N^T L^{-1} M \in \mathbb{R}^{2ms(p+1) \times 2ms(p+1)}$ is a bit more involved than before. With abuse of notation, we start by recalling that the vector $e_j \in \mathbb{R}^{2ms(p+1)}$, $j = 1, \dots, 2ms(p+1)$, can be written as $e_j = \text{vec}(e_k e_h^T)$, $e_k \in \mathbb{R}^{2m(p+1)}$, $e_h \in \mathbb{R}^s$, $j = k + 2m(p+1) \cdot (h-1)$. Therefore,

$$\begin{aligned} e_i^T N^T L^{-1} M e_j &= \text{vec}(e_r e_q^T)^T N^T L^{-1} M \text{vec}(e_k e_h^T) \\ &= \text{vec}(e_r e_q^T \boldsymbol{\alpha}_s [e_{\ell-s+1}, \dots, e_\ell]^T \mathcal{F}^{-1})^T L^{-1} \text{vec}(e_k e_h^T [e_1, \dots, e_s]^T \mathcal{F}^T) \\ &= \text{vec}(e_r e_q^T \boldsymbol{\alpha}_s [e_{\ell-s+1}, \dots, e_\ell]^T \mathcal{F}^{-1})^T \text{vec}(\mathcal{H} \odot (e_k e_h^T \mathcal{F}^T)) \\ &= \langle \mathcal{H} \odot (e_k e_h^T \mathcal{F}^T), e_r e_q^T \boldsymbol{\alpha}_s [e_{\ell-s+1}, \dots, e_\ell]^T \mathcal{F}^{-1} \rangle_F \\ &= \text{trace}(\mathcal{F}^{-T}[e_{\ell-s+1}, \dots, e_\ell] \boldsymbol{\alpha}_s^T e_q e_r^T (\mathcal{H} \odot (e_k e_h^T \mathcal{F}^T))) \\ &= e_r^T (\mathcal{H} \odot (e_k e_h^T \mathcal{F}^T)) \mathcal{F}^{-T}[e_{\ell-s+1}, \dots, e_\ell] \boldsymbol{\alpha}_s^T e_q. \end{aligned}$$

Notice that in the second step above we have $e_h^T [e_1, \dots, e_s]^T = e_h^T$ and, differently from the one in the left-hand side where $e_h \in \mathbb{R}^s$, the vector in the right-hand side denotes the h -th canonical basis vector of \mathbb{R}^ℓ , $h = 1, \dots, s$.

By exploiting the same property of the Hadamard product used in the derivation presented in section 4.2, we have

$$(4.18) \quad \begin{aligned} e_i^T N^T L^{-1} M e_j &= \text{trace}(\text{diag}(e_r) \mathcal{H} \text{diag}(\mathcal{F}^{-T}[e_{\ell-s+1}, \dots, e_\ell] \boldsymbol{\alpha}_s^T e_q) \mathcal{F} e_h e_k^T) \\ &= e_k^T \text{diag}(e_r) \mathcal{H} (\mathcal{F}^{-T}[e_{\ell-s+1}, \dots, e_\ell] \boldsymbol{\alpha}_s^T e_q) \odot \mathcal{F} e_h \\ &= \delta_{k,r} e_r^T \mathcal{H} (\mathcal{F}^{-T}[e_{\ell-s+1}, \dots, e_\ell] \boldsymbol{\alpha}_s^T e_q) \odot \mathcal{F} e_h. \end{aligned}$$

Recalling that the indices in the above expression are such that $i = r + 2m(p+1) \cdot (q-1)$ and $j = k + 2m(p+1) \cdot (h-1)$, the relation in (4.18) means that $N^T L^{-1} M$ is a $s \times s$ block matrix with blocks of size $2m(p+1)$ which are all diagonal. The (q, h) -th block of $N^T L^{-1} M$ is given by $\text{diag}(\mathcal{H}(\mathcal{F}^{-T}[e_{\ell-s+1}, \dots, e_\ell] \alpha_s^T e_q) \odot \mathcal{F} e_h)$.

If $\mathcal{S} := I + N^T L^{-1} M$ and $Z := \mathcal{H} \odot (S_m^{-1} E_1 \gamma(\mathcal{F}[e_1, \tau \beta F_2])^T)$, then we denote by P the $2m(p-1) \times s$ matrix such that $\text{vec}(P) = \mathcal{S}^{-1} \text{vec}(Z \mathcal{F}^{-T}[e_{\ell-s+1}, \dots, e_\ell] \alpha_s^T)$ and, to conclude, the solution Y_m of the reduced problems (4.16) can be computed by

$$(4.19) \quad Y_m = S_m(Z - W) \mathcal{F}^{-T}, \quad \text{where} \quad \begin{aligned} Z &= \mathcal{H} \odot (S_m^{-1} E_1 \gamma(\mathcal{F}[e_1, \tau \beta F_2])^T), \\ W &= \mathcal{H} \odot (P[e_1, \dots, e_s]^T \mathcal{F}^T). \end{aligned}$$

A generic BDF of order s , $s \leq 6$, requires $s-1$ additional initial values $\mathbf{u}_1, \dots, \mathbf{u}_{s-1}$ together with \mathbf{u}_0 . If these values are known, we have to simply change the right-hand side in (4.15) and consider $[\sum_{j=1}^s \alpha_j \mathbf{u}_{s-j}, \sum_{j=1}^{s-1} \alpha_{j+1} \mathbf{u}_{s-j}, \dots, \alpha_s \mathbf{u}_{s-1}, F_1][e_1, e_2, \dots, e_s, \tau \beta F_2]^T$ in place of $[\mathbf{u}_0, F_1][e_1, \tau \beta F_2]^T$. Therefore, we need to construct the space $\mathbf{E} \mathbf{K}_m^\square(\bar{K}_d, [\sum_{j=1}^s \alpha_j \mathbf{u}_{s-j}, \sum_{j=1}^{s-1} \alpha_{j+1} \mathbf{u}_{s-j}, \dots, \alpha_s \mathbf{u}_{s-1}, F_1])$. Except for the fact that now $2(p+s)$ basis vectors are added to the computed space at each iteration, the main steps of the solution method remain the same. See Example 7.1.

If $\mathbf{u}_1, \dots, \mathbf{u}_{s-1}$ are not given, they must be carefully approximated and such a computation must be $\mathcal{O}(\tau^s)$ accurate to maintain the full convergence order of the method. In standard implementation of BDFs, the k -th initial value \mathbf{u}_k , $k = 1, \dots, s-1$, is computed by a BDF of order k with a time-step τ_k , $\tau_k \leq \tau$. See, e.g., [1, Section 5.1.3]. Allowing for a variable time-stepping is crucial for preserving the convergence order of the method.

The solution scheme presented in this paper is designed for a uniform time grid and it is not able to automatically handle a variable time-stepping. Therefore, even though the solution process is illustrated for a generic BDF of order $s \leq 6$, in the experiments reported in section 7 we make use of the implicit Euler scheme for the time discretization when the additional initial values $\mathbf{u}_1, \dots, \mathbf{u}_{s-1}$ are not provided.

The generalization of the proposed algorithm to the case of variable, and more in general, adaptive time-stepping will be the topic of future works.

5. The rational Krylov subspace method. In section 4 we have considered only the extended Krylov subspace for the projection of the discrete space operator. However, the framework presented in section 4.1 can be easily adapted to handle different approximation spaces as, e.g., the rational Krylov subspace (1.4).

If we need to solve equation (3.5), we can construct the rational Krylov subspace $\mathbf{K}_m^\square(\bar{K}_d, [\mathbf{u}_0, F_1], \boldsymbol{\xi}) = \text{Range}(V_m)$, $V_m = [\mathcal{V}_1, \dots, \mathcal{V}_m] \in \mathbb{R}^{n \times m(p+1)}$, $\boldsymbol{\xi} = (\xi_2, \dots, \xi_m)^T \in \mathbb{C}^{m-1}$, and perform a left projection as illustrated in section 4.1. Therefore, we still look for an approximate solution U_m of the form $U_m = V_m Y_m$ where $Y_m \in \mathbb{R}^{m(p+1) \times m(p+1)}$ is computed by imposing a Galerkin condition on the residual matrix $R_m := (\bigotimes_{i=1}^d (I - \mathcal{P}_1) + \tau \bar{K}_d) V_m Y_m - V_m Y_m \Sigma_1^T - [\mathbf{u}_0, F_1][e_1, \tau F_2]^T$, i.e., we impose $V_m^T R_m = 0$. Once again, this orthogonality condition is equivalent to computing Y_m as the solution of the projected equation

$$(\mathcal{I}_m + \tau T_m) Y_m - Y_m \Sigma_1^T = E_1 \gamma[e_1, \tau F_2]^T,$$

where, as before, $T_m = V_m^T \bar{K}_d V_m$ and $\mathcal{I}_m = V_m^T \left(\bigotimes_{i=1}^d (I - \mathcal{P}_1) \right) V_m$. Also when the rational Krylov subspace is selected as approximation space we perform an explicit projection to obtain T_m and \mathcal{I}_m although, in exact arithmetic, the matrix T_m can be computed by exploiting the results in [10, Proposition 4.1]. The solution Y_m to the reduced equation can be still calculated by (4.12).

Even though the main framework is similar to the one derived in section 4, the employment of a rational Krylov subspace requires the careful implementation of certain technical aspects that we are going to discuss in the following.

The basis V_m can be computed by an Arnoldi-like procedure as illustrated in [10, Section 2] and it is well-known how the quality of the computed rational Krylov subspace deeply depends on the choice of the shifts $\boldsymbol{\xi}$ employed in the basis construction. Effective shifts can be computed at the beginning of the iterative method if, e.g., some additional informations about the problem of interest are known. In practice, the shifts can be adaptively computed on the fly and the strategy presented in [10] can be employed to calculate the $(m+1)$ -th shift ξ_{m+1} . The adaptive procedure proposed by Druskin and Simoncini in [10] only requires rough estimates of the smallest and largest eigenvalues of \bar{K}_d together with the Ritz values, i.e., the eigenvalues

of the projected matrix T_m , that can be efficiently computed in $\mathcal{O}(m^3(p+1)^3)$ flops. In all the examples reported in section 7 such a scheme is adopted for the shifts computation.

For the rational Krylov subspace, the residual norm cannot be computed by performing (4.3) as an Arnoldi relation of the form

$$\overline{K}_d V_m = V_m T_m + \mathcal{V}_{m+1} E_{m+1}^T \underline{T}_m,$$

does not hold. An alternative but still cheap residual norm computation is derived in the next proposition.

PROPOSITION 5.1. *At the m -th iteration of the rational Krylov subspace method, the residual matrix $R_m = (\bigotimes_{i=1}^d (I - \mathcal{P}_1) + \tau \overline{K}_d) V_m Y_m - V_m Y_m \Sigma_1^T - [\mathbf{u}_0, F_1][e_1, \tau F_2]^T$ is such that*

$$\|R_m\|_F = \tau \left\| (\xi_{m+1} I - (I - V_m V_m^T) \overline{K}_d) \mathcal{V}_{m+1} E_{m+1}^T \underline{H}_m H_m^{-1} Y_m \right\|_F,$$

where the matrix $\underline{H}_m \in \mathbb{R}^{(m+1) \cdot (p+1) \times m(p+1)}$ collects the orthonormalization coefficients stemming from the “rational” Arnoldi procedure and $H_m \in \mathbb{R}^{m(p+1) \times m(p+1)}$ is its principal square submatrix.

Proof. For the rational Krylov subspace $\mathbf{K}_m^\square(\overline{K}_d, [\mathbf{u}_0, F_1], \xi) = \text{Range}(V_m)$, $V_m = [\mathcal{V}_1, \dots, \mathcal{V}_m]$, the following Arnoldi-like relation holds

$$(5.1) \quad \overline{K}_d V_m = V_m T_m + \mathcal{V}_{m+1} E_{m+1}^T \underline{H}_m (\text{diag}(\xi_2, \dots, \xi_{m+1}) \otimes I_{p+1}) H_m^{-1} - (I - V_m V_m^T) \overline{K}_d \mathcal{V}_{m+1} E_{m+1}^T \underline{H}_m H_m^{-1}.$$

See, e.g., [10, 34]. Since the Arnoldi procedure is employed in the basis construction, \underline{H}_m is a block upper Hessenberg matrix with block of size $p+1$ and we can write

$$E_{m+1}^T \underline{H}_m (\text{diag}(\xi_2, \dots, \xi_{m+1}) \otimes I_{p+1}) = \xi_{m+1} E_{m+1}^T \underline{H}_m.$$

The residual matrix R_m is such that

$$\begin{aligned} R_m &= \left(\bigotimes_{i=1}^d (I - \mathcal{P}_1) + \tau \overline{K}_d \right) V_m Y_m - V_m Y_m \Sigma_1^T - [\mathbf{u}_0, F_1][e_1, \tau F_2]^T \\ &= V_m ((\mathcal{I}_m + \tau T_m) Y_m - Y_m \Sigma_1^T - E_1 \boldsymbol{\gamma}[e_1, \tau F_2]^T) \\ &\quad + \tau (\mathcal{V}_{m+1} E_{m+1}^T \underline{H}_m (\text{diag}(\xi_2, \dots, \xi_{m+1}) \otimes I_{p+1}) H_m^{-1} - (I - V_m V_m^T) \overline{K}_d \mathcal{V}_{m+1} E_{m+1}^T \underline{H}_m H_m^{-1}) Y_m \\ &= \tau (\xi_{m+1} \mathcal{V}_{m+1} E_{m+1}^T \underline{H}_m H_m^{-1} - (I - V_m V_m^T) \overline{K}_d \mathcal{V}_{m+1} E_{m+1}^T \underline{H}_m H_m^{-1}) Y_m, \end{aligned}$$

and collecting the matrix $\mathcal{V}_{m+1} E_{m+1}^T \underline{H}_m H_m^{-1}$ we get the result. \square

Proposition 5.1 shows how the convergence check requires to compute the Frobenius norm of a $n \times m(p+1)$ matrix when the rational Krylov subspace is employed. This operation can be carried out in $\mathcal{O}(nm(p+1))$ flops by exploiting the cyclic property of the trace operator.

If $d = 2, 3$ and the initial values u_0 , the source term f and the boundary conditions g are separable functions in the space variables, the same strategy presented in section 4.1.1 can be adopted also when the rational Krylov subspace is selected in place of the extended one. We can compute d rational Krylov subspaces corresponding to d subspaces of \mathbb{R}^n instead of one rational Krylov subspace contained in \mathbb{R}^{n^d} . Results similar to the one in Proposition 4.1 can be derived by combining the arguments in the proof of Proposition 4.1 with the Arnoldi-like relation (5.1).

In this section we have assumed that the implicit Euler scheme is employed for the time integration. Some modifications are necessary to handle BDFs of higher order and the resulting scheme can be easily derived by following the discussion in section 4.3.

6. The convection-diffusion equation. In principle, the matrix reformulation presented in section 2, and thus the solution process illustrated in section 4-5, can be applied to any PDEs of the form $u_t + \mathfrak{L}(u) = f$ where only space derivatives are involved in the linear differential operator \mathfrak{L} .

In this section we provide some details in the case of the time-dependent convection-diffusion equation

$$(6.1) \quad \begin{aligned} u_t - \varepsilon \Delta u + \vec{w} \cdot \nabla u &= f, & \text{in } \Omega \times (0, T], \\ u &= g, & \text{on } \partial\Omega, \\ u(x, 0) &= u_0(x), \end{aligned}$$

where $\Omega \subset \mathbb{R}^d$ is regular, $\varepsilon > 0$ is the viscosity parameter and the convection vector $\vec{w} = \vec{w}(x)$ is assumed to be incompressible, i.e., $\text{div}(\vec{w}) = 0$.

As already mentioned, if $K_d^{\text{cd}} \in \mathbb{R}^{n^d \times n^d}$ denotes the matrix stemming from the discretization of the convection-diffusion operator $\mathfrak{L}(u) = -\varepsilon \Delta u + \vec{w} \cdot \nabla u$ on $\bar{\Omega}$, the same exact arguments of section 2 lead to the Sylvester matrix equation

$$(I_{n^d} + \tau K_d^{\text{cd}})\mathbf{U} - \mathbf{U}\Sigma_1^T = [\mathbf{u}_0, F_1][e_1, \tau F_2],$$

when the backward Euler scheme is employed for the time integration.

If $d = 1$ and $\vec{w} = \phi(x)$, the matrix K_1^{cd} can be written as $K_1^{\text{cd}} = \varepsilon K_1 + \Phi B_1$ where, as before, K_1 denotes the discrete negative laplacian whereas B_1 represents the discrete first derivative and the diagonal matrix Φ collects the nodal values $\phi(x_i)$ on its diagonal.

In [31], it has been shown that the 2- and 3D discrete convection-diffusion operators possess a Kronecker structure if the components of \vec{w} are separable functions in the space variables.

If $\vec{w} = (\phi_1(x)\psi_1(y), \phi_2(x)\psi_2(y))$ and Φ_i, Ψ_i are diagonal matrices collecting on the diagonal the nodal values of the corresponding functions $\phi_i, \psi_i, i = 1, 2$, then

$$(6.2) \quad K_2^{\text{cd}} = \varepsilon K_1 \otimes I + \varepsilon I \otimes K_1 + \Psi_1 \otimes \Phi_1 B_1 + \Psi_2 B_1 \otimes \Phi_2.$$

See [31, Proposition 1]. Analogously, if $d = 3$ and $\vec{w} = (\phi_1(x)\psi_1(y)v_1(z), \phi_2(x)\psi_2(y)v_2(z), \phi_3(x)\psi_3(y)v_3(z))$, we can write

$$(6.3) \quad K_3^{\text{cd}} = \varepsilon K_1 \otimes I \otimes I + \varepsilon I \otimes K_1 \otimes I + \varepsilon I \otimes I \otimes K_1 + \Psi_1 \otimes \Upsilon_1 \otimes \Phi_1 B_1 + \Psi_2 B_1 \otimes \Upsilon_2 \otimes \Phi_2 + \Psi_3 \otimes \Upsilon_3 B_1 \otimes \Phi_3.$$

where, as before, the diagonal matrices $\Phi_i, \Psi_i, \Upsilon_i$ collect on the main diagonal the nodal values of the corresponding functions. See [31, Proposition 2].

In this case, we can take advantage of the Kronecker structure of K_d^{cd} to automatically include the boundary conditions in the matrix equation formulation of the time-dependent convection-diffusion equation. This can be done by combining the arguments of section 3 with the strategy presented in [31, Section 3].

Even though K_d^{cd} still has a Kronecker structure, this cannot be exploited in general for reducing the cost of the basis generation for $d = 2, 3$ as it has been described in section 4.1.1, also when u_0, f and g are separable functions in the space variables. This is due to the presence of the extra terms containing B_1 in the definitions (6.2)-(6.3) of K_d^{cd} . Indeed, K_d^{cd} is no longer of the form $\sum_{i=1}^d I \otimes \dots \otimes I \otimes A_i \otimes I \otimes \dots \otimes I$ and the tensorized Krylov approach presented in [20] cannot be employed. This difficulty is strictly related to the fact that efficient projection methods for generic generalized Sylvester equations of the form

$$\sum_{j=1}^p A_j X B_j = C_1 C_2^T,$$

have not been developed so far. The available methods work well if the coefficient matrices A_i and B_i fulfill certain assumptions which may be difficult to meet in case of the discrete convection-diffusion operator. See, e.g. [3, 18, 33, 37] for more details about solvers for generalized matrix equations.

The matrix K_d^{cd} can be expressed as $\sum_{i=1}^d I \otimes \dots \otimes I \otimes A_i \otimes I \otimes \dots \otimes I$ in some very particular cases. For instance, if $d = 2$ and $\vec{w} = (\phi(x), \psi(y))$, then

$$K_2^{\text{cd}} = (\varepsilon K_1 + \Psi B_1) \otimes I + I \otimes (\varepsilon K_1 + \Phi B_1).$$

Therefore, if $\mathbf{u}_0 = \phi_{u_0} \otimes \psi_{u_0}$ and $[\mathbf{f}_1, \dots, \mathbf{f}_\ell] = F_1 F_2^T = (\Phi_f \otimes \Psi_f) F_2^T$, the spaces $\mathbf{EK}_m^\square(\varepsilon K_1 + \Psi B_1, [\phi_{u_0}, \Phi_f])$ and $\mathbf{EK}_m^\square(\varepsilon K_1 + \Phi B_1, [\psi_{u_0}, \Psi_f])$ can be constructed in place of $\mathbf{EK}_m^\square(K_2^{\text{cd}}, [\mathbf{u}_0, F_1])$. Similarly if the rational Krylov subspace is employed as approximation space.

7. Numerical results. In this section we compare our new matrix equation approach with state-of-the-art procedures for the solution of the algebraic problem arising from the discretization of time-dependent PDEs. Different solvers can be applied to (2.2) depending on how one interprets the underlying structure of the linear operator \mathcal{A} . We reformulate (2.2) as a matrix equation but clearly \mathcal{A} can be seen as a large structured matrix and well-known iterative techniques as, e.g., GMRES [36], can be employed in the solution

of the linear system (2.2). The matrix \mathcal{A} does not need to be explicitly assembled and its Kronecker structure can be exploited to perform “matrix-vector” products. Moreover, one should take advantage of the low-rank of the right-hand side $\text{vec}([\mathbf{u}_0, F_1][e_1, \tau F_2]^T)$ to reduce the memory consumption of the procedure. Indeed, if $n^d \ell$ is very large, we would like to avoid the allocation of any long $n^d \ell$ dimensional vectors and this can be done by rewriting the Krylov iteration in matrix form and equipping the Arnoldi procedure with a couple of low-rank truncations. These variants of Krylov schemes are usually referred to as low-rank Krylov methods and in the following we will apply low-rank GMRES (LR-GMRES) to the solution of (2.2). See, e.g., [3, 6, 17] for some low-rank Krylov procedures applied to the solution of linear matrix equations while [23] for details about how to preserve the convergence properties of the Krylov routines when low-rank truncations are performed.

Both the aforementioned variants of GMRES needs to be preconditioned to achieve a fast convergence in terms of number of iterations. In [27], it has been shown that the operator

$$\begin{aligned} \mathfrak{P} : \mathbb{R}^{n^d \ell} &\rightarrow \mathbb{R}^{n^d \ell} \\ x &\mapsto (I_\ell \otimes (I_{n^d} + \tau K_d) - C_1 \otimes I_{n^d})x, \end{aligned}$$

is a good preconditioner for (2.2). If right preconditioning is adopted, at each iteration of the selected Krylov procedure we have to solve an equation of the form $\mathfrak{P}\hat{v} = v_m$, where v_m denotes the last basis vector that has been computed. Again, many different procedures can be employed for this task. In case of GMRES, we invert \mathfrak{P} by applying the algebraic multigrid method AGMG developed by Notay and coauthors [28–30]. The employment of AGMG in the inversion of \mathfrak{P} requires the explicit construction of both the matrix $I_\ell \otimes (I_{n^d} + \tau K_d) - C_1 \otimes I_{n^d}$ and the basis vector $v_m \in \mathbb{R}^{n^d \ell}$, therefore we cannot apply AGMG in the framework of low-rank Krylov techniques as we would lose all the benefits coming from the low-rank truncations. Since $\mathfrak{P}\hat{v} = v_m$ can be recast in terms of a matrix equation, in case of LR-GMRES we can inexactly invert \mathfrak{P} by applying few iterations of Algorithm 4.1. Notice that in this case, due to the definition of \mathfrak{P} , the solution of the inner equations in Algorithm 4.1 is easier. Indeed, with the notation of section 4.2, we have $Y_m = S_m Z \mathcal{F}^{-T}$ at each iteration m . However, since the extra computational efforts of computing Y_m by (4.12) turned out to be very moderate with respect to the cost of performing $Y_m = S_m Z \mathcal{F}^{-T}$, we decided to run few iterations of Algorithm 4.1 with the original operator instead of the preconditioner \mathfrak{P} . This procedure can be seen as an inner-outer Krylov scheme [41].

To try to reduce the cost of the preconditioning step, we perform (at most) 10 iterations of AGMG and Algorithm 4.1 at each outer iteration.

The preconditioning techniques adopted within GMRES and LR-GMRES are all nonlinear. We thus have to employ flexible variants of the outer Krylov routines, namely FGMRES [35] and LR-FGMRES.

We would like to underline that the concept of preconditioner does not really exist in the context of matrix equations. See, e.g., [40, Section 4.4]. The efficiency of our novel approach mainly relies on the effectiveness of the selected approximation space.

In the following we will denote our matrix equation approach by either EKSM, when the extended Krylov subspace is adopted, or RKSM, if the rational Krylov subspace is employed as approximation space. The construction of both the extended Krylov subspace $\mathbf{EK}_m^\square(\bar{K}_d, [\mathbf{u}_0, F_1])$ and the rational Krylov subspace $\mathbf{K}_m^\square(\bar{K}_d, [\mathbf{u}_0, F_1], \boldsymbol{\xi})$ requires the solution of linear systems with the coefficient matrix \bar{K}_d (or a shifted version of it). Except for Example 7.4, these linear solves are carried out by means of the Matlab sparse direct solver *backslash*. In particular, for EKSM, the LU factors of \bar{K}_d are computed once and for all at the beginning of the iterative procedure so that only triangular systems are solved during the basis construction. The time for such LU decomposition is always included in the reported results.

To sum up, we are going to compare EKSM and RKSM with FGMRES preconditioned by AGMG (FGMRES+AGMG) and LR-FGMRES preconditioned by EKSM (LR-FGMRES+EKSM). The performances of the different algorithms are compared in terms of both computational time and memory requirements. In particular, since all the methods we compare need to allocate the basis of a certain Krylov subspace, the storage demand of each algorithm consists of the dimension of the computed subspace. The memory requirements of the adopted schemes are summarized in Table 7.1 where m indicates the number of performed iterations.

For LR-FGMRES, r_i and z_i denote the rank of the low-rank matrix representing the i -th vector of the unpreconditioned and preconditioned basis respectively.

Notice that for separable problems where the strategy presented in section (4.1.1) can be applied, the

Table 7.1: Storage demand of the compared methods.

| EKSM | RKSM | FGMRES | LR-FGMRES |
|-----------------------|----------------------|-------------|-----------------------------------------|
| $2m(p+1)(n^d + \ell)$ | $m(p+1)(n^d + \ell)$ | $2mn^d\ell$ | $(n^d + \ell) \sum_{i=1}^m (r_i + z_i)$ |

memory requirements of EKSM and RKSM can be reduced to $2m \sum_{i=1}^d p_i n + 2^d m^d \prod_{i=1}^d p_i \ell$ and $m \sum_{i=1}^d p_i n + m^d \prod_{i=1}^d p_i \ell$ respectively, where p_i denotes the rank of the initial block used in the construction of the i -th Krylov subspace, $i = 1, \dots, d$.

If not stated otherwise, the tolerance of the final relative residual norm is always set to 10^{-6} .

All results were obtained with Matlab R2017b [26] on a machine with 2.1 GHz processors and 192GB of RAM.

EXAMPLE 7.1. Before comparing EKSM and RKSM with other solvers we would like to show first how our novel reformulation of the algebraic problem in terms of a Sylvester matrix equation is able to maintain the convergence order of the adopted discretization schemes. In particular, we present only the results obtained by EKSM as the ones achieved by applying RKSM are very similar.

We consider the following 1D problem

$$(7.1) \quad \begin{aligned} u_t &= \Delta u, & \text{in } (0, \pi) \times (0, 1], \\ u(0) = u(\pi) &= 0, \\ u(x, 0) &= \sin(x). \end{aligned}$$

This is a toy problem as the exact solution is known in closed form and it is given by $u(x, t) = \sin(x)e^{-t}$. With u at hand, we are able to calculate the discretization error provided by our solution process.

Equation (7.1) is discretized by means of second order centered finite differences in space and a BDF of order s , $s \leq 6$, in time.

In the following we denote by $U_m \in \mathbb{R}^{n \times \ell}$ the approximate solution computed by EKSM, by U the $n \times \ell$ matrix whose i -th column represents the exact solution evaluated on the space nodal values at time t_i whereas $\mathbf{U} \in \mathbb{R}^{n \times \ell}$ collects the ℓ vectors computed by sequentially solving the linear systems in (2.1) by backslash.

We first solve the algebraic problem by EKSM with a tolerance $\epsilon = 10^{-10}$ and we compare the obtained U_m with \mathbf{U} . In Table 7.2 we report the results for $n = 4096$, $s = 1$ and different values of ℓ .

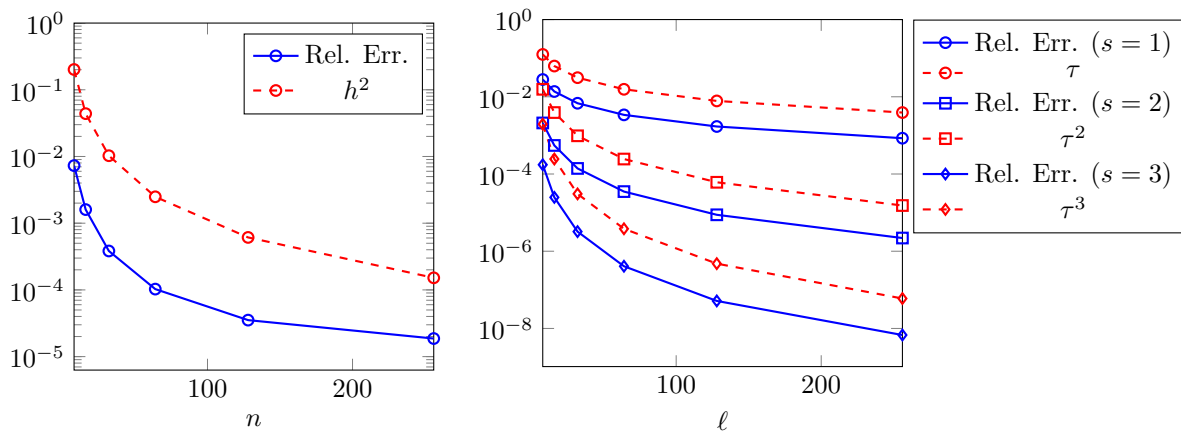
Table 7.2: Example 7.1. Results for different values of ℓ . $n = 4096$, $s = 1$.

| ℓ | EKSM | | backslash | $\ U_m - \mathbf{U}\ _F / \ \mathbf{U}\ _F$ |
|--------|------|-------------|-------------|---------------------------------------------|
| | It. | Time (secs) | Time (secs) | |
| 1024 | 2 | 4.891e-2 | 5.697e-1 | 2.009e-10 |
| 4096 | 2 | 6.094e-2 | 2.501e0 | 1.0066e-10 |
| 16384 | 2 | 8.647e-2 | 9.912e0 | 9.931e-11 |
| 65536 | 2 | 1.737e-1 | 3.964e1 | 1.069e-11 |

Looking at the timings reported in Table 7.2, since EKSM requires two iterations to convergence for all the tested values of ℓ , we can readily appreciate how the computational cost of our novel approach mildly depends on ℓ while the time for the sequential solution of the linear systems in (2.1) linearly grows with the number of time steps.

Moreover, we see how, for this example, we can obtain a very small algebraic error $\|U_m - \mathbf{U}\|_F / \|\mathbf{U}\|_F$ by setting a strict tolerance on the relative residual norm computed by EKSM. This means that, when we compare U_m with U , the discretization error is the quantity that contributes the most to $\|U_m - U\|_F / \|U\|_F$. In Figure 7.1 we plot $\|U_m - U\|_F / \|U\|_F$ for different values of n , ℓ and s . In particular, in the picture on the left we plot the relative error for $\ell = 16384$ and $s = 1$ while varying n . On the right, we fix $n = 32768$ and we

Fig. 7.1: Example 7.1. $\|U_m - U\|_F / \|U\|_F$ for different values of n , ℓ and s . Left: $\ell = 16384$, $s = 1$ while n varies (h denotes the space mesh size). Right: $n = 32768$, $s = 1, 2, 3$ while ℓ varies.



plot $\|U_m - U\|_F / \|U\|_F$ for different values of ℓ and $s = 1, 2, 3$. Notice that by knowing the analytic expression of the solution u , for $s > 1$ we are able to provide the $s - 1$ additional initial conditions $\mathbf{u}_1, \dots, \mathbf{u}_{s-1}$ and the extended Krylov subspace $\mathbf{EK}_m^\square(\bar{K}_1, [\sum_{j=1}^s \alpha_j \mathbf{u}_{s-j}, \sum_{j=1}^{s-1} \alpha_{j+1} \mathbf{u}_{s-j}, \dots, \alpha_s \mathbf{u}_{s-1}])$ can be constructed as discussed in section 4.3.

From the plots in Figure 7.1 we can recognize how the convergence order of the tested discretization schemes is always preserved. Similar results are obtained for larger values of s , namely $s = 4, 5, 6$, provided either a larger n or a space discretization scheme with a larger convergence order is employed.

EXAMPLE 7.2. In the second example we consider the same equation presented in [27, Section 6.1]. This consists in the following 2D heat equation

$$(7.2) \quad \begin{aligned} u_t &= \Delta u, & \text{in } \Omega \times (0, 1], \quad \Omega := (0, 1)^2, \\ u &= 0, & \text{on } \partial\Omega, \\ u_0 = u(x, y, 0) &= x(x-1)y(y-1). \end{aligned}$$

Equation (7.2) is discretized by means of second order centered finite differences in space and the backward Euler scheme in time.

Since the initial condition is a separable function in the space variables, and both the source term and the boundary conditions are zero, the strategy presented in section 4.1.1 can be adopted. In particular if \mathbf{u}_0 denotes the n^2 vector collecting the values of u_0 for all the nodal values (x_i, y_j) , then we can write $\mathbf{u}_0 = \boldsymbol{\phi}_{u_0} \otimes \boldsymbol{\psi}_{u_0}$ where $\boldsymbol{\phi}_{u_0} = [x_1(x_1 - 1), \dots, x_n(x_n - 1)]^T$, $\boldsymbol{\psi}_{u_0} = [y_1(y_1 - 1), \dots, y_n(y_n - 1)]^T \in \mathbb{R}^n$. Therefore, the two extended Krylov subspaces $\mathbf{EK}_m^\square(\bar{K}_1, \boldsymbol{\phi}_{u_0})$ and $\mathbf{EK}_m^\square(\bar{K}_1, \boldsymbol{\psi}_{u_0})$ can be constructed in place of $\mathbf{EK}_m^\square(\bar{K}_2, \mathbf{u}_0)$. Similarly for the rational Krylov subspace method.

In Table 7.3 we report the results for different values of n and ℓ .

We can notice that the number of iterations computed by FGMRES+AGMG varies a lot for different problem settings. This is probably due to the approximate application of \mathfrak{P}^{-1} . For some problem dimensions the setting we employed led to an inadequate preconditioning phase with a consequent increment in the outer iteration count. A more accurate tuning of AGMG may be beneficial for the overall solution procedure. However, also when FGMRES+AGMG needs few iterations to converge, its computational time is not comparable with the ones achieved by the other routines. Moreover, for $n = 128$ and $\ell = 16384$, FGMRES+AGMG did not converge in 50 (outer) iterations and we thus stopped the process, whereas for the largest problem dimensions we tested, the system returned an *Out of Memory* (OOM) message when we tried to assemble the matrix \mathfrak{P} .

LR-FGMRES+EKSM performs quite well in terms of computational time, especially for small n , and the number of iterations needed to converge is rather independent of both n and ℓ confirming the quality of the preconditioning technique.

Table 7.3: Example 7.2. Results for different values of n and ℓ .

| n | ℓ | EKSM | | RKSM | | FGMRES+AGMG | | LR-FGMRES+EKSM | |
|-----|--------|------|-------------|------|-------------|-------------|-------------|----------------|-------------|
| | | It. | Time (secs) | It. | Time (secs) | It. | Time (secs) | It. | Time (secs) |
| 64 | 1024 | 6 | 2.487e-1 | 9 | 3.313e-1 | 19 | 1.461e2 | 1 | 1.899e-1 |
| | 4096 | 6 | 4.209e-1 | 9 | 3.140e-1 | 3 | 8.102e1 | 1 | 1.747e-1 |
| | 16384 | 6 | 6.182e-1 | 9 | 5.913e-1 | 2 | 2.694e2 | 1 | 3.020e-1 |
| | 65536 | 6 | 1.671e0 | 9 | 1.783e0 | 1 | 6.863e2 | 2 | 4.001e0 |
| 128 | 1024 | 7 | 2.989e-1 | 11 | 3.629e-1 | 8 | 2231e2 | 2 | 2.476e0 |
| | 4096 | 8 | 4.449e-1 | 11 | 4.252e-1 | 8 | 9.483e2 | 2 | 2.624e0 |
| | 16384 | 7 | 1.426e0 | 11 | 1.089e0 | – | – | 2 | 2.595e0 |
| | 65536 | 7 | 2.480e0 | 10 | 2.349e0 | OoM | OoM | 2 | 5.584e0 |
| 256 | 1024 | 8 | 4.071e-1 | 11 | 3.887e-1 | 12 | 1.445e3 | 2 | 1.992e1 |
| | 4096 | 10 | 9.726e-1 | 13 | 5.540e-1 | 27 | 1.856e5 | 2 | 1.980e1 |
| | 16384 | 10 | 1.916e0 | 13 | 1.401e0 | OoM | OoM | 2 | 2.141e1 |
| | 65536 | 10 | 5.469e0 | 11 | 2.895e0 | OoM | OoM | 2 | 1.654e1 |

Our new algorithms, EKSM and RKSM, are very fast. We would like to remind the reader that, for this example, the number of degrees of freedom (DoF) is equal to $n^2\ell$. This means that, for the finest refinement of the space and time grids we tested, our routines are able to solve a problem with $\mathcal{O}(4 \cdot 10^9)$ DoF in few seconds while reaching the desired accuracy.

The number of iterations performed by EKSM and RKSM turns out to be very robust with respect to ℓ and the (almost) constant iteration count we obtain for a fixed n lets us appreciate once more how the computational cost of our procedures modestly grows with ℓ .

The robustness of our routines with respect to n is not surprising. Indeed, the projection procedure we perform only involves the spatial component of the overall operator, namely $\bigotimes_{i=1}^2(I_n - \mathcal{P}_1) - \tau \bar{K}_2$, and its effectiveness thus strictly depends on the spectral properties of $\bigotimes_{i=1}^2(I_n - \mathcal{P}_1) - \tau \bar{K}_2$ which are mainly fixed for a given n although the mild dependence on ℓ due to the presence of the scalar τ .

Thanks to the separability of equation (7.2) and the employment of the strategy presented in section 4.1.1, EKSM and RKSM are very competitive also in terms of storage demand as illustrated in Table 7.4.

Table 7.4: Example 7.2. Memory requirements of the compared methods for different values of n and ℓ .

| n | ℓ | EKSM | RKSM | FGMRES+AGMG | LR-FGMRES+EKSM |
|-----|--------|---------------|---------------|-------------|------------------|
| 64 | 1024 | $24n+144\ell$ | $18n+81\ell$ | $38n^2\ell$ | $18(n^2 + \ell)$ |
| | 4096 | $24n+144\ell$ | $18n+81\ell$ | $6n^2\ell$ | $18(n^2 + \ell)$ |
| | 16384 | $24n+144\ell$ | $18n+81\ell$ | $4n^2\ell$ | $18(n^2 + \ell)$ |
| | 65536 | $24n+144\ell$ | $18n+81\ell$ | $2n^2\ell$ | $80(n^2 + \ell)$ |
| 128 | 1024 | $28n+196\ell$ | $22n+121\ell$ | $16n^2\ell$ | $84(n^2 + \ell)$ |
| | 4096 | $32n+256\ell$ | $22n+121\ell$ | $16n^2\ell$ | $84(n^2 + \ell)$ |
| | 16384 | $32n+256\ell$ | $22n+121\ell$ | – | $85(n^2 + \ell)$ |
| | 65536 | $28n+196\ell$ | $20n+100\ell$ | OoM | $86(n^2 + \ell)$ |
| 256 | 1024 | $32n+256\ell$ | $22n+121\ell$ | $24n^2\ell$ | $87(n^2 + \ell)$ |
| | 4096 | $40n+400\ell$ | $26n+169\ell$ | $54n^2\ell$ | $89(n^2 + \ell)$ |
| | 16384 | $40n+400\ell$ | $26n+169\ell$ | OoM | $90(n^2 + \ell)$ |
| | 65536 | $40n+400\ell$ | $22n+121\ell$ | OoM | $90(n^2 + \ell)$ |

EXAMPLE 7.3. We consider another example coming from [27]. In particular, the problem we address is

the following time-dependent convection-diffusion equation

$$(7.3) \quad \begin{aligned} u_t - \varepsilon \Delta u + \vec{w} \cdot \nabla u &= 0, & \text{in } \Omega \times (0, 1], \quad \Omega := (0, 1)^2, \\ u &= g(x, y), & \text{on } \partial\Omega, \\ u_0 = u(x, y, 0) &= g(x, y) & \text{if } (x, y) \in \partial\Omega, \\ u_0 = u(x, y, 0) &= 0 & \text{otherwise,} \end{aligned}$$

where $\vec{w} = (2y(1-x^2), -2x(1-y^2))$ and $g(1, y) = g(x, 0) = g(x, 1) = 0$ while $g(0, y) = 1$.

This is a simple model for studying how the temperature in a cavity with a (constant) ‘‘hot’’ external wall ($\{0\} \times [0, 1]$) distributes over time. The wind characterized by \vec{w} determines a recirculating flow.

Once again, equation (7.3) is discretized by means of second order centered finite differences in space and the backward Euler scheme in time.

Thanks to the separability of \vec{w} , the spatial discrete operator \bar{K}_2^{cd} has a Kronecker structure and it can be written as in (6.2). However, the presence of the extra terms containing the discrete first order derivative operator does not allow for the memory-saving strategy described in section 4.1.1. Nevertheless, the structure of \bar{K}_2^{cd} can be exploited to easily include the boundary conditions in the matrix equation formulation. Moreover, since the initial condition is equal to the boundary conditions on the boundary nodes and zero otherwise, the boundary conditions do not depend on time, and the source term is zero everywhere, the right-hand side of equation (3.5) can be written as $[\mathbf{u}_0, F_1][e_1, \tau[0, \mathbf{1}_{\ell-1}]^T]^T$ where, with a notation similar to the one used in section 3, $F_1 \in \mathbb{R}^{n^2}$ is such that $\mathcal{P}_2(\mathbf{u}_0 e_1^T + \tau F_1 [0, \mathbf{1}_{\ell-1}]^T) = \mathcal{L}_2^{\text{cd}} \mathbf{U}$ on the boundary nodes and zero otherwise. $\mathbf{1}_{\ell-1} \in \mathbb{R}^{\ell-1}$ denotes the vector of all ones.

Therefore, EKSM and RKSM construct the spaces $\mathbf{EK}_m^\square(\bar{K}_2^{\text{cd}}, [\mathbf{u}_0, F_1])$ and $\mathbf{K}_m^\square(\bar{K}_2^{\text{cd}}, [\mathbf{u}_0, F_1], \boldsymbol{\xi})$ respectively.

In Table 7.5 we report the results for different values of n , ℓ and the viscosity parameter ε .

From the values in Table 7.5 we can readily notice how this is a very difficult problem for FGMRES+AGMG especially for small ε when FGMRES+AGMG seldom converges in less than 50 iterations.

LR-FGMRES+EKSM is very competitive in terms of running time as long as very few outer iterations are needed to converge. Indeed, its computational cost per iteration is not fixed but grows quite remarkably as the outer iterations proceed. This is mainly due to the preconditioning step. At each LR-FGMRES iteration k , EKSM is applied to an equation whose right-hand side is given by the low-rank matrix that represents the k -th basis vector of the computed space and the rank of such a matrix grows with k . This significantly increases the computational efforts needed to perform the 10 EKSM iterations prescribed as preconditioning step worsening the performance of the overall solution procedure.

Also for this example, the new routines we propose in this paper perform quite well and the number of iterations mildly depends on ℓ .

The performances of our solvers are also pretty robust with respect to ε and, especially for RKSM, it turns out that the number of iterations needed to converge gets smaller as the value of ε is reduced. In the steady-state setting, this phenomenon is well-understood. See, e.g., [12, Section 4.2.2]. In our framework, we can explain such a trend by adapting convergence results for RKSM applied to Lyapunov equations. Indeed, in [9, Theorem 4.2] it is shown how the convergence of RKSM for Lyapunov equations is guided by the maximum value of a certain rational function over the field of values $W(A) := \{z^* A z, z \in \mathbb{C}^n, \|z\| = 1\}$ of the matrix A used to define the employed rational Krylov subspace. Roughly speaking, the smaller $W(A)$, the better. In our context, even though we use \bar{K}_2^{cd} to build $\mathbf{K}_m^\square(\bar{K}_2^{\text{cd}}, [\mathbf{u}_0, F_1], \boldsymbol{\xi})$, the projection technique involves the whole coefficient matrix $\bigotimes_{i=1}^2 (I_n - \mathcal{P}_1) - \tau \bar{K}_2^{\text{cd}}$ and we thus believe it is reasonable to think that the success of RKSM relies on the field of values of such a matrix. In Figure 7.2 we plot the field of values of $\bigotimes_{i=1}^2 (I_n - \mathcal{P}_1) - \tau \bar{K}_2^{\text{cd}}$ for $n = 256$, $\ell = 1024$, and different values of ε and we can appreciate how such sets are nested and they get smaller when decreasing ε . This may intuitively explain the relation between the RKSM iteration count and ε but further studies in this direction are necessary.

Even though the approach presented in section 4.1.1 cannot be adopted in this example, EKSM and RKSM are still very competitive also in terms of storage demand as illustrated in Table 7.6.

We conclude this example by showing that our routines are also able to identify the physical properties of the continuous solution we want to approximate. In Figure 7.3 we report the solution computed by EKSM for the case $n = 256$ and $\ell = 1024$. In particular, we report the solution at different time steps $t_1, t_{\ell/2}, t_\ell$ (left to right) and for different values of ε (top to bottom). We remind the reader that our solution represents

Table 7.5: Example 7.3. Results for different values of n , ℓ and ε .

| ε | n | ℓ | EKSM | | RKSM | | FGMRES+AGMG | | LR-FGMRES+EKSM | |
|---------------|-----|--------|------|-------------|------|-------------|-------------|-------------|----------------|-------------|
| | | | It. | Time (secs) | It. | Time (secs) | It. | Time (secs) | It. | Time (secs) |
| 1 | 64 | 1024 | 13 | 3.977e-1 | 24 | 1.186e0 | 21 | 1.601e2 | 3 | 3.014e0 |
| | | 4096 | 14 | 3.459e-1 | 25 | 1.322e0 | 7 | 1.972e2 | 2 | 1.529e0 |
| | | 16384 | 14 | 8.421e-1 | 23 | 1.613e0 | 3 | 3.965e2 | 2 | 3.427e0 |
| | | 65536 | 13 | 2.333e0 | 24 | 3.908e0 | 3 | 2.346e3 | 2 | 7.437e0 |
| | 128 | 1024 | 15 | 2.072e0 | 26 | 4.584e0 | 23 | 7.515e2 | 2 | 5.995e0 |
| | | 4096 | 18 | 2.947e0 | 27 | 4.365e0 | 28 | 4.448e3e3 | 2 | 6.847e0 |
| | | 16384 | 19 | 2.830e0 | 28 | 5.571e0 | - | - | 2 | 8.445e0 |
| | | 65536 | 18 | 5.208e0 | 28 | 7.472e0 | OoM | OoM | 2 | 1.272e1 |
| | 256 | 1024 | 17 | 1.720e1 | 32 | 2.709e1 | 45 | 6.836e3 | 2 | 3.669e1 |
| | | 4096 | 21 | 2.027e1 | 38 | 3.338e1 | 35 | 2.418e4 | 2 | 4.613e1 |
| | | 16384 | 24 | 2.426e1 | 39 | 3.507e1 | OoM | OoM | 3 | 1.187e2 |
| | | 65536 | 25 | 2.081e1 | 38 | 3.552e1 | OoM | OoM | 3 | 1.330e2 |
| 0.1 | 64 | 1024 | 15 | 5.347e-1 | 22 | 1.277e0 | 10 | 7.253e1 | 2 | 1.291e0 |
| | | 4096 | 14 | 4.380e-1 | 23 | 1.174e0 | 6 | 1.775e2 | 2 | 1.367e0 |
| | | 16384 | 14 | 9.353e-1 | 23 | 1.678e0 | 4 | 5.223e2 | 2 | 2.662e0 |
| | | 65536 | 13 | 2.447e0 | 20 | 2.922e0 | 4 | 3.406e3 | 2 | 6.083e0 |
| | 128 | 1024 | 20 | 2.256e0 | 27 | 4.769e0 | 16 | 4.892e2e2 | 2 | 5.465e0 |
| | | 4096 | 20 | 2.107e0 | 27 | 4.605e0 | 14 | 1.793e3 | 2 | 5.009e0 |
| | | 16384 | 19 | 2.977e0 | 24 | 4.084e0 | 23 | 1.676e4 | 2 | 6.881e0 |
| | | 65536 | 19 | 5.593e0 | 26 | 7.043e0 | OoM | OoM | 3 | 5.314e1 |
| | 256 | 1024 | 25 | 2.261e1 | 35 | 2.821e1 | 38 | 5.553e3 | 3 | 1.002e2 |
| | | 4096 | 27 | 1.607e1 | 32 | 2.261e1 | - | - | 3 | 8.767e1 |
| | | 16384 | 26 | 1.623e1 | 31 | 2.492e1 | OoM | OoM | 3 | 1.023e2 |
| | | 65536 | 25 | 2.062e1 | 30 | 2.417e1 | OoM | OoM | 3 | 1.836e2 |
| 0.01 | 64 | 1024 | 10 | 2.126e-1 | 16 | 7.507e-1 | 33 | 2.813e2 | 2 | 1.055e0 |
| | | 4096 | 9 | 2.509e-1 | 18 | 9.415e-1 | - | - | 2 | 9.823e-1 |
| | | 16384 | 9 | 4.855e-1 | 18 | 1.235e0 | 8 | 1.281e3 | 2 | 1.778e0 |
| | | 65536 | 10 | 1.536e0 | 20 | 2.467e0 | 7 | 7.173e3 | 2 | 5.878e0 |
| | 128 | 1024 | 13 | 1.333e0 | 18 | 2.590e0 | - | - | 2 | 4.022e0 |
| | | 4096 | 12 | 1.304e0 | 20 | 2.679e0 | - | - | 2 | 3.841e0 |
| | | 16384 | 12 | 1.579e0 | 22 | 3.453e0 | - | - | 2 | 4.876e0 |
| | | 65536 | 12 | 2.951e0 | 20 | 4.575e0 | OoM | OoM | 2 | 7.809e0 |
| | 256 | 1024 | 19 | 1.255e1 | 24 | 1.508e1 | - | - | 2 | 2.823e1 |
| | | 4096 | 18 | 1.166e1 | 25 | 1.727e1 | - | - | 2 | 2.658e1 |
| | | 16384 | 17 | 1.261e1 | 25 | 1.815e1 | OoM | OoM | 2 | 2.662e1 |
| | | 65536 | 17 | 1.393e1 | 22 | 1.382e1 | OoM | OoM | 4 | 1.448e2 |

the temperature distribution in a cavity with a constant, hot external wall. Looking at Figure 7.3, we can appreciate how the temperature distributes quite evenly in our domain for $\varepsilon = 1$. The smaller ε , the more viscous the media our temperature spreads in. Therefore, the temperature is different from zero only in a very restricted area of our domain, close to the hot wall, for $\varepsilon = 0.1, 0.01$. Notice that for $\varepsilon = 0.01$ and t_1 , the part of the domain where the temperature is nonzero is so narrow that is difficult to appreciate with the resolution of Figure 7.3. For $\varepsilon = 0.1, 0.01$ we can also see how the temperature stops being evenly distributed as for $\varepsilon = 1$ but follows the circulating flow defined by the convection vector \vec{w} .

EXAMPLE 7.4. For the last example, we take inspiration from [31, Example 5] and consider the following 3D time-dependent convection-diffusion equation

$$\begin{aligned}
 (7.4) \quad u_t - \Delta u + \vec{w} \cdot \nabla u &= 0, \quad \text{in } \Omega \times (0, 1], \quad \Omega := (0, 1)^3, \\
 u &= 0, \quad \text{on } \partial\Omega, \\
 u_0 &= g,
 \end{aligned}$$

Fig. 7.2: Example 7.3. Field of values of $\bigotimes_{i=1}^2 (I_n - \mathcal{P}_1) - \tau \overline{K}_2^{\text{cd}}$ for $n = 64$, $\ell = 1024$ and different ε .

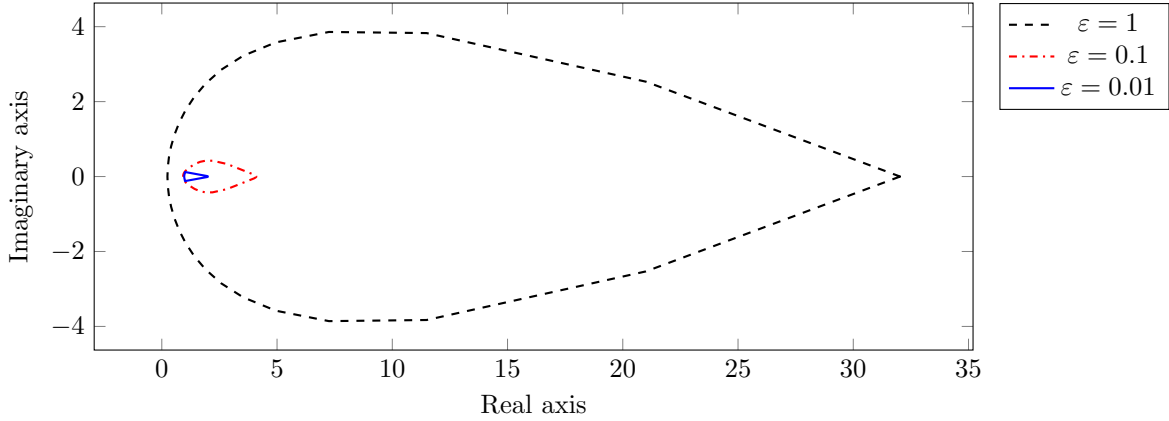
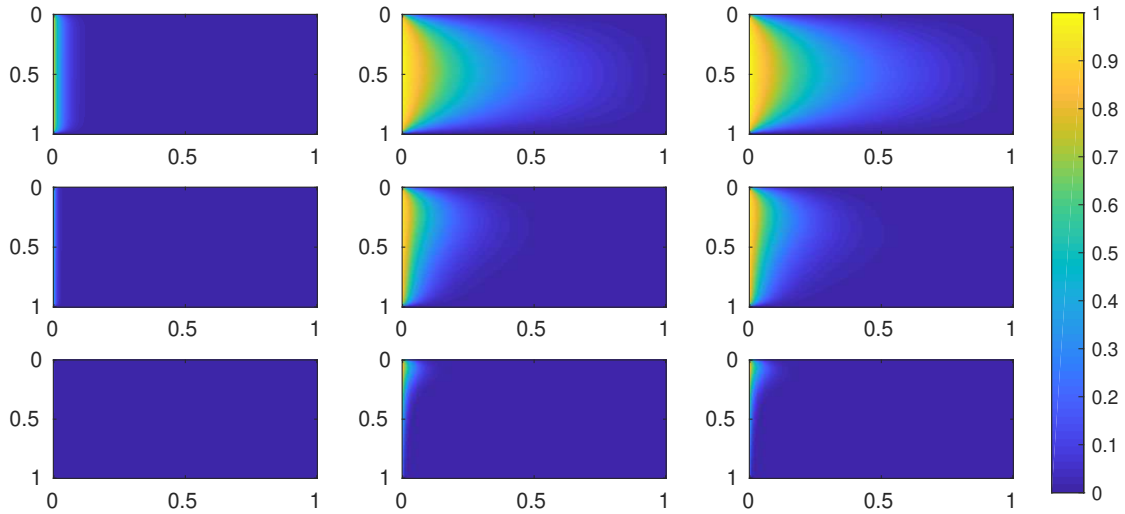


Fig. 7.3: Example 7.3. Computed solution at different time steps (left to right: t_1 , $t_{\ell/2}$, t_ℓ) and related to different values of ε (top to bottom: $\varepsilon = 1$, $\varepsilon = 0.1$, $\varepsilon = 0.01$). $n = 256$, $\ell = 1024$.



where $\vec{w} = (x \sin x, y \cos y, e^{z^2-1})$ and g is such that

$$(7.5) \quad \begin{aligned} -\Delta g + \vec{w} \cdot \nabla g &= 1, & \text{in } \Omega, \\ g &= 0, & \text{on } \partial\Omega. \end{aligned}$$

Both (7.4) and (7.5) are discretized by centered finite differences in space and the backward Euler scheme is used for the time integration of (7.4). Once (7.5) is discretized, we compute a numerical solution $\mathbf{g} \in \mathbb{R}^{n^3}$ by applying the strategy presented in, e.g., [31], and then set $\mathbf{u}_0 = \mathbf{g}$.

Also in this example the convection vector \vec{w} is a separable function in the space variables and the stiffness matrix $\overline{K}_3^{\text{cd}} \in \mathbb{R}^{n^3 \times n^3}$ can be written in terms of a Kronecker sum as illustrated in section 6. However, the initial value \mathbf{u}_0 is not separable in general and we have to employ $\mathbf{EK}_m^\square(\overline{K}_3^{\text{cd}}, \mathbf{u}_0)$ and $\mathbf{K}_m^\square(\overline{K}_3^{\text{cd}}, \mathbf{u}_0, \boldsymbol{\xi})$ as approximation spaces.

It is well-known how sparse direct routines are not very well suited for solving linear systems with a coefficient matrix that stems from the discretization of a 3D differential operator, and iterative methods

Table 7.6: Example 7.3. Memory requirements of the compared methods for different values of n , ℓ and ε .

| ε | n | ℓ | EKSM | RKSM | FGMRES+AGMG | LR-FGMRES+EKSM |
|---------------|-----|--------|-------------------|------------------|-------------|--------------------|
| 1 | 64 | 1024 | $52(n^2 + \ell)$ | $48(n^2 + \ell)$ | $42n^2\ell$ | $659(n^2 + \ell)$ |
| | | 4096 | $56(n^2 + \ell)$ | $50(n^2 + \ell)$ | $14n^2\ell$ | $324(n^2 + \ell)$ |
| | | 16384 | $56(n^2 + \ell)$ | $46(n^2 + \ell)$ | $6n^2\ell$ | $323(n^2 + \ell)$ |
| | | 65536 | $52(n^2 + \ell)$ | $48(n^2 + \ell)$ | $6n^2\ell$ | $234(n^2 + \ell)$ |
| | 128 | 1024 | $60(n^2 + \ell)$ | $52(n^2 + \ell)$ | $46n^2\ell$ | $325(n^2 + \ell)$ |
| | | 4096 | $72(n^2 + \ell)$ | $54(n^2 + \ell)$ | $56n^2\ell$ | $372(n^2 + \ell)$ |
| | | 16384 | $76(n^2 + \ell)$ | $56(n^2 + \ell)$ | – | $379(n^2 + \ell)$ |
| | | 65536 | $72(n^2 + \ell)$ | $56(n^2 + \ell)$ | OoM | $332(n^2 + \ell)$ |
| | 256 | 1024 | $68(n^2 + \ell)$ | $64(n^2 + \ell)$ | $90n^2\ell$ | $327(n^2 + \ell)$ |
| | | 4096 | $84(n^2 + \ell)$ | $76(n^2 + \ell)$ | $70n^2\ell$ | $402(n^2 + \ell)$ |
| | | 16384 | $96(n^2 + \ell)$ | $78(n^2 + \ell)$ | OoM | $1102(n^2 + \ell)$ |
| | | 65536 | $100(n^2 + \ell)$ | $76(n^2 + \ell)$ | OoM | $1293(n^2 + \ell)$ |
| 0.1 | 64 | 1024 | $60(n^2 + \ell)$ | $44(n^2 + \ell)$ | $20n^2\ell$ | $330(n^2 + \ell)$ |
| | | 4096 | $56(n^2 + \ell)$ | $46(n^2 + \ell)$ | $12n^2\ell$ | $302(n^2 + \ell)$ |
| | | 16384 | $56(n^2 + \ell)$ | $46(n^2 + \ell)$ | $8n^2\ell$ | $259(n^2 + \ell)$ |
| | | 65536 | $52(n^2 + \ell)$ | $40(n^2 + \ell)$ | $8n^2\ell$ | $167(n^2 + \ell)$ |
| | 128 | 1024 | $80(n^2 + \ell)$ | $54(n^2 + \ell)$ | $32n^2\ell$ | $381(n^2 + \ell)$ |
| | | 4096 | $80(n^2 + \ell)$ | $54(n^2 + \ell)$ | $28n^2\ell$ | $362(n^2 + \ell)$ |
| | | 16384 | $76(n^2 + \ell)$ | $48(n^2 + \ell)$ | $46n^2\ell$ | $356(n^2 + \ell)$ |
| | | 65536 | $76(n^2 + \ell)$ | $52(n^2 + \ell)$ | OoM | $1198(n^2 + \ell)$ |
| | 256 | 1024 | $100(n^2 + \ell)$ | $70(n^2 + \ell)$ | $76n^2\ell$ | $955(n^2 + \ell)$ |
| | | 4096 | $108(n^2 + \ell)$ | $64(n^2 + \ell)$ | – | $1108(n^2 + \ell)$ |
| | | 16384 | $104(n^2 + \ell)$ | $62(n^2 + \ell)$ | OoM | $1213(n^2 + \ell)$ |
| | | 65536 | $100(n^2 + \ell)$ | $60(n^2 + \ell)$ | OoM | $1662(n^2 + \ell)$ |
| 0.01 | 64 | 1024 | $40(n^2 + \ell)$ | $32(n^2 + \ell)$ | $66n^2\ell$ | $275(n^2 + \ell)$ |
| | | 4096 | $36(n^2 + \ell)$ | $36(n^2 + \ell)$ | – | $228(n^2 + \ell)$ |
| | | 16384 | $36(n^2 + \ell)$ | $36(n^2 + \ell)$ | $16n^2\ell$ | $160(n^2 + \ell)$ |
| | | 65536 | $40(n^2 + \ell)$ | $40(n^2 + \ell)$ | $14n^2\ell$ | $161(n^2 + \ell)$ |
| | 128 | 1024 | $52(n^2 + \ell)$ | $36(n^2 + \ell)$ | – | $302(n^2 + \ell)$ |
| | | 4096 | $48(n^2 + \ell)$ | $40(n^2 + \ell)$ | – | $279(n^2 + \ell)$ |
| | | 16384 | $48(n^2 + \ell)$ | $44(n^2 + \ell)$ | – | $259(n^2 + \ell)$ |
| | | 65536 | $48(n^2 + \ell)$ | $40(n^2 + \ell)$ | OoM | $168(n^2 + \ell)$ |
| | 256 | 1024 | $76(n^2 + \ell)$ | $24(n^2 + \ell)$ | – | $361(n^2 + \ell)$ |
| | | 4096 | $72(n^2 + \ell)$ | $50(n^2 + \ell)$ | – | $334(n^2 + \ell)$ |
| | | 16384 | $68(n^2 + \ell)$ | $50(n^2 + \ell)$ | OoM | $292(n^2 + \ell)$ |
| | | 65536 | $68(n^2 + \ell)$ | $44(n^2 + \ell)$ | OoM | $1659(n^2 + \ell)$ |

perform better most of the time. Therefore, the inner-outer GMRES method is employed to solve the linear systems involved in the basis construction of both $\mathbf{EK}_m^\square(\overline{K}_3^{\text{cd}}, \mathbf{u}_0)$ and $\mathbf{K}_m^\square(\overline{K}_3^{\text{cd}}, \mathbf{u}_0, \boldsymbol{\xi})$. We set the tolerance on the relative residual norm for such linear systems equal to 10^{-8} , i.e., two order of magnitude less than the outer tolerance. However, the novel results about inexact procedures in the basis construction of the rational and extended Krylov subspace presented in [22] may be adopted to further reduce the computational cost

of our schemes.

Due to the very large number $n^3\ell$ of DoFs we employ, in Table 7.7 we report only the results for EKSM and RKSM.

Table 7.7: Example 7.4. Results for different values of n and ℓ .

| n | ℓ | EKSM | | | RKSM | | |
|-----|--------|------|-------------|------------------|------|-------------|------------------|
| | | It. | Time (secs) | Mem. | It. | Time (secs) | Mem. |
| 32 | 1024 | 10 | 1.026e1 | $20(n^3 + \ell)$ | 12 | 5.158e0 | $12(n^3 + \ell)$ |
| | 4096 | 10 | 1.029e1 | $20(n^3 + \ell)$ | 13 | 6.121e0 | $13(n^3 + \ell)$ |
| | 16384 | 10 | 1.705e1 | $20(n^3 + \ell)$ | 13 | 5.479e0 | $13(n^3 + \ell)$ |
| | 65536 | 10 | 2.371e1 | $20(n^3 + \ell)$ | 12 | 5.385e0 | $12(n^3 + \ell)$ |
| 64 | 1024 | 12 | 8.367e1 | $24(n^3 + \ell)$ | 15 | 4.378e1 | $15(n^3 + \ell)$ |
| | 4096 | 13 | 9.287e1 | $26(n^3 + \ell)$ | 16 | 4.326e1 | $16(n^3 + \ell)$ |
| | 16384 | 13 | 9.109e1 | $26(n^3 + \ell)$ | 15 | 4.296e1 | $15(n^3 + \ell)$ |
| | 65536 | 12 | 1.595e2 | $26(n^3 + \ell)$ | 15 | 4.356e1 | $15(n^3 + \ell)$ |
| 128 | 1024 | 16 | 1.143e3 | $32(n^3 + \ell)$ | 18 | 4.631e2 | $18(n^3 + \ell)$ |
| | 4096 | 18 | 1.293e3 | $36(n^3 + \ell)$ | 19 | 4.855e2 | $19(n^3 + \ell)$ |
| | 16384 | 18 | 1.298e3 | $36(n^3 + \ell)$ | 18 | 4.541e2 | $18(n^3 + \ell)$ |
| | 65536 | 17 | 1.237e3 | $34(n^3 + \ell)$ | 16 | 3.915e2 | $16(n^3 + \ell)$ |

We can appreciate how our routines need a very reasonable time to meet the prescribed accuracy while maintaining a moderate storage consumption. For instance, the finest space and time grids we consider lead to a problem with $\mathcal{O}(10^{11})$ DoFs and RKSM manages to converge in few minutes by constructing a very low dimensional subspace.

It is interesting to notice how the computational time of RKSM is always much smaller than the one achieved by EKSM. This is due to the difference in the time devoted to the solution of the linear systems during the basis construction. Indeed, in RKSM, shifted linear systems of the form $\bar{K}_3^{\text{gd}} - \xi_j I$ have to be solved and, in this example, it turns out that GMRES is able to achieve the prescribed accuracy in terms of relative residual norm in much fewer iterations than what it is able to do when solving linear systems with the only \bar{K}_3^{gd} as it is done in EKSM.

8. Conclusions. In this paper we have shown how the discrete operator stemming from the discretization of time-dependent PDEs can be described in terms of a matrix equation. For sake of simplicity, we have restricted our discussion to the heat equation and evolutionary convection-diffusion equations, but the same strategy can be applied to any PDE of the form $u_t + \mathfrak{L}(u) = f$ whenever $\mathfrak{L}(u)$ is a linear differential operator involving only space derivatives, provided certain assumptions on the source term f and the boundary conditions are fulfilled.

The matrix equation formulation of the discrete problem naturally encodes the separability of the spatial and time derivatives of the underlying differential operator. This lets us employ different strategies to deal with the spatial and time components of the algebraic problem and combine them in a very efficient solution procedure. In particular, timely projection techniques have been proposed to tackle the spatial operator while the entry-wise structure of the time discrete operator has been exploited to derive effective solution schemes.

We have shown how to fully exploit the possible Kronecker structure of the stiffness matrix. Very good results are obtained also when this structure is not capitalized on in the solution process. This means that our approach can be successfully applied also to problems which do not lead to a stiffness matrix that possesses a Kronecker form as, e.g., in case of spatial domains Ω with a complex geometry or when sophisticated discretization methods (in space) are employed. We believe that also elaborate space-time adaptive techniques [8, 24] can benefit from our novel approach. In particular, our routines can be employed to efficiently address the linear algebra phase within adaptive schemes for fixed time and space grids. Once the

grids have been modified, our solvers can deal with the discrete operator defined on the newly generated time-space meshes. Both EKSM and RKSM can be easily implemented and we believe they can be incorporated in state-of-the-art software packages like, e.g., KARDOS [13].

As already mentioned, in the proposed approach the time step size τ is assumed to be fixed. We plan to extend our algorithm to the case of adaptive time-stepping discretization schemes in the near future.

Acknowledgments. We wish to thank Peter Benner, Jens Saak and Valeria Simoncini for insightful comments on earlier versions of the manuscript. Their helpful suggestions are greatly appreciated.

The author is a member of the Italian INdAM Research group GNCS.

REFERENCES

- [1] U. M. ASCHER AND L. R. PETZOLD, *Computer methods for ordinary differential equations and differential-algebraic equations*, Society for Industrial and Applied Mathematics (SIAM), Philadelphia, PA, 1998.
- [2] R. H. BARTELS AND G. W. STEWART, *Algorithm 432: Solution of the Matrix Equation $AX + XB = C$* , *Comm. ACM*, 15 (1972), pp. 820–826.
- [3] P. BENNER AND T. BREITEN, *Low rank methods for a class of generalized Lyapunov equations and related issues*, *Numer. Math.*, 124 (2013), pp. 441–470.
- [4] P. BENNER, M. KÖHLER, AND J. SAAK, *Sparse-dense Sylvester equations in \mathcal{H}_2 -model order reduction*, Tech. Report MPIMD/11-11, Max Planck Institute Magdeburg, 2011.
- [5] P. BENNER AND P. KÜRSCHNER, *Computing real low-rank solutions of Sylvester equations by the factored ADI method*, *Comput. Math. Appl.*, 67 (2014), pp. 1656–1672.
- [6] T. BREITEN, V. SIMONCINI, AND M. STOLL, *Low-rank solvers for fractional differential equations*, *Electron. Trans. Numer. Anal.*, 45 (2016), pp. 107–132.
- [7] M. C. D’AUTILIA, I. SGURA, AND V. SIMONCINI, *Matrix-oriented discretization methods for reaction-diffusion PDEs: comparisons and applications*, (2019). Preprint, ArXiv: 1903.05030.
- [8] P. DEUFLHARD AND M. WEISER, *Adaptive numerical solution of PDEs*, De Gruyter Textbook, Walter de Gruyter & Co., Berlin, 2012.
- [9] V. DRUSKIN, L. KNIZHNERMAN, AND V. SIMONCINI, *Analysis of the rational Krylov subspace and ADI methods for solving the Lyapunov equation*, *SIAM J. Numer. Anal.*, 49 (2011), pp. 1875–1898.
- [10] V. DRUSKIN AND V. SIMONCINI, *Adaptive rational Krylov subspaces for large-scale dynamical systems*, *Systems Control Lett.*, 60 (2011), pp. 546–560.
- [11] V. DRUSKIN, V. SIMONCINI, AND M. ZASLAVSKY, *Adaptive tangential interpolation in rational Krylov subspaces for MIMO dynamical systems*, *SIAM J. Matrix Anal. Appl.*, 35 (2014), pp. 476–498.
- [12] H. C. ELMAN, D. J. SILVESTER, AND A. J. WATHEN, *Finite elements and fast iterative solvers: with applications in incompressible fluid dynamics*, Numerical Mathematics and Scientific Computation, Oxford University Press, Oxford, second ed., 2014.
- [13] B. ERDMANN, J. LANG, AND R. ROITZSCH, *KARDOS - User’s Guide*, Tech. Report 02-42, ZIB, Takustr. 7, 14195 Berlin, 2002.
- [14] G. H. GOLUB, S. NASH, AND C. VAN LOAN, *A Hessenberg-Schur method for the problem $AX + XB = C$* , *IEEE Trans. Automat. Control*, 24 (1979), pp. 909–913.
- [15] G. H. GOLUB AND C. F. VAN LOAN, *Matrix computations*, Johns Hopkins Studies in the Mathematical Sciences, Johns Hopkins University Press, Baltimore, MD, fourth ed., 2013.
- [16] M. H. GUTKNECHT, *Krylov subspace algorithms for systems with multiple right hand sides: an introduction*, in Modern mathematical models, methods and algorithms for real world systems, A. H. Siddiqi, I. Duff, and O. Christensen, eds., Anshan Ltd, 2007. Available at <http://www.sam.math.ethz.ch/~mhg/pub/delhipap.pdf>.
- [17] M. HOCHBRUCK AND G. STARKE, *Preconditioned Krylov subspace methods for Lyapunov matrix equations*, *SIAM J. Matrix Anal. Appl.*, 16 (1995), pp. 156–171.
- [18] E. JARLEBRING, G. MELE, D. PALITTA, AND E. RINGH, *Krylov methods for low-rank commuting generalized sylvester equations*, *Numerical Linear Algebra with Applications*, 25 (2018). e2176.
- [19] L. KNIZHNERMAN AND V. SIMONCINI, *Convergence analysis of the extended Krylov subspace method for the Lyapunov equation*, *Numer. Math.*, 118 (2011), pp. 567–586.
- [20] D. KRESSNER AND C. TOBLER, *Krylov subspace methods for linear systems with tensor product structure*, *SIAM J. Matrix Anal. Appl.*, 31 (2009/10), pp. 1688–1714.
- [21] ———, *Low-rank tensor Krylov subspace methods for parametrized linear systems*, *SIAM J. Matrix Anal. Appl.*, 32 (2011), pp. 1288–1316.
- [22] P. KÜRSCHNER AND M. FREITAG, *Inexact methods for the low rank solution to large scale Lyapunov equations*, (2018). ArXiv preprint: 1809.06903.
- [23] P. KÜRSCHNER AND D. PALITTA, *On the convergence of low-rank Krylov methods*, (2019). In preparation.
- [24] J. LANG, *Adaptive multilevel solution of nonlinear parabolic PDE systems*, vol. 16 of Lecture Notes in Computational Science and Engineering, Springer-Verlag, Berlin, 2001. Theory, algorithm, and applications.
- [25] T. MACH AND J. SAAK, *Towards an ADI iteration for tensor structured equations*, Tech. Report MPIMD/11-12, Max Planck Institute Magdeburg, 2011.
- [26] MATLAB, *version 9.3.0 (R2017b)*, The MathWorks Inc., Natick, Massachusetts, 2017.
- [27] E. McDONALD, J. PESTANA, AND A. WATHEN, *Preconditioning and iterative solution of all-at-once systems for evolutionary partial differential equations*, *SIAM J. Sci. Comput.*, 40 (2018), pp. A1012–A1033.

- [28] A. NAPOV AND Y. NOTAY, *An algebraic multigrid method with guaranteed convergence rate*, SIAM J. Sci. Comput., 34 (2012), pp. A1079–A1109.
- [29] Y. NOTAY, *An aggregation-based algebraic multigrid method*, Electron. Trans. Numer. Anal., 37 (2010), pp. 123–146.
- [30] ———, *Aggregation-based algebraic multigrid for convection-diffusion equations*, SIAM J. Sci. Comput., 34 (2012), pp. A2288–A2316.
- [31] D. PALITTA AND V. SIMONCINI, *Matrix-equation-based strategies for convection-diffusion equations*, BIT, 56 (2016), pp. 751–776.
- [32] D. PALITTA AND V. SIMONCINI, *Computationally enhanced projection methods for symmetric Sylvester and Lyapunov equations*, J. Comput. Appl. Math., 330 (2018), pp. 648–659.
- [33] C. E. POWELL, D. SILVESTER, AND V. SIMONCINI, *An efficient reduced basis solver for stochastic Galerkin matrix equations*, SIAM J. Sci. Comput., 39 (2017), pp. A141–A163.
- [34] A. RUHE, *The rational Krylov algorithm for nonsymmetric eigenvalue problems. III: complex shifts for real matrices*, BIT, Vol. 34 (1994), pp. pp. 165–176.
- [35] Y. SAAD, *A flexible inner-outer preconditioned GMRES algorithm*, SIAM J. Sci. Comput., 14 (1993), pp. 461–469.
- [36] Y. SAAD AND M. H. SCHULTZ, *GMRES: a generalized minimal residual algorithm for solving nonsymmetric linear systems*, SIAM J. Sci. Statist. Comput., 7 (1986), pp. 856–869.
- [37] S. D. SHANK, V. SIMONCINI, AND D. B. SZYLD, *Efficient low-rank solution of generalized Lyapunov equations*, Numer. Math., 134 (2016), pp. 327–342.
- [38] V. SIMONCINI, *A new iterative method for solving large-scale Lyapunov matrix equations*, SIAM J. Sci. Comput., 29 (2007), pp. 1268–1288.
- [39] ———, *Extended Krylov subspace for parameter dependent systems*, Appl. Numer. Math., 60 (2010), pp. 550–560.
- [40] ———, *Computational methods for linear matrix equations*, SIAM Rev., 58 (2016), pp. 377–441.
- [41] V. SIMONCINI AND D. B. SZYLD, *Flexible inner-outer Krylov subspace methods*, SIAM J. Numer. Anal., 40 (2002), pp. 2219–2239 (2003).
- [42] G. STARKE, *Optimal alternating direction implicit parameters for nonsymmetric systems of linear equations*, SIAM J. Numer. Anal., 28 (1991), pp. 1431–1445.
- [43] E. L. WACHSPRESS, *Extended application of alternating direction implicit iteration model problem theory*, J. Soc. Indust. Appl. Math., 11 (1963), pp. 994–1016.
- [44] ———, *Generalized ADI preconditioning*, Comput. Math. Appl., 10 (1984), pp. 457–461 (1985).